The Thesis Committee for Juliana Jennifer Spector
Certifies that this is the approved version of the following thesis:

Feedbacks between dissolution, abrasion, and bed roughness: A flume investigation of carbonate bedrock incision

APPROVED BY
SUPERVISING COMMITTEE:

Supervisor:

Joel Johnson

James Buttles

Wonsuck Kim

Feedbacks between dissolution, abrasion, and bed roughness: A flume investigation of carbonate bedrock incision

by

Juliana Jennifer Spector

Thesis

Presented to the Faculty of the Graduate School of

The University of Texas at Austin

in Partial Fulfillment

of the Requirements

for the Degree of

Master of Science in Geological Sciences

The University of Texas at Austin

December 2017

Dedication

I dedicate this work to my parents, family, and friends who inspired and supported me in finishing this thesis.

Acknowledgements

I would like to thank my adviser, Joel Johnson, for his encouragement and guidance throughout the research process. I am grateful to him especially for being enthusiastic and willing to take me on as a student in my second year of the Master's program and helping me to complete this thesis in a timely manner and achieve my academic goals.

I would also like to acknowledge Jim Buttles for loaning me equipment in the lab, taking an interest in my project, and assisting me whenever he could. In addition, I thank Jim for serving on my committee and for the helpful feedback on my thesis writing.

Additionally, I want to extend thanks to Wonsuck Kim for serving me as a committee member and for his constructive comments on the thesis. Thank you also to Muhammad Ashraf for his assistance with pouring the plaster that served as the flume bed for the experiments. Finally, this research was conducted at The University of Texas at Austin Morphodynamics Laboratory in the Center for Water in the Environment, and I thank the principal investigators, staff, postdocs, and fellow graduate researchers for graciously allowing me to work in and share this space.

On a personal note, I am appreciative to my friends at the Jackson School of Geosciences and the College Houses Halstead Cooperative who have helped fuel my passion for science and given me the confidence to persevere through research challenges.

Abstract

Feedbacks between dissolution, abrasion, and bed roughness: A flume investigation of carbonate bedrock incision

Juliana Jennifer Spector, MSGeoSci

The University of Texas at Austin, 2017

Supervisor: Joel Johnson

Traditionally, the chemical dissolution and erosion of bedrock in eroding river channels has been viewed as minor to negligible in comparison to mechanical weathering processes, such as impact wear from transported bedload sediment. However, for relatively soluble rocks, such as carbonates and evaporites, dissolution could be a significant contributor to erosion. The motivation for this project is to understand controls on the relative importance of bedrock dissolution and abrasion under different lithological and hydrological conditions. I hypothesize that physical and chemical erosion will cause subsequent increases in bed roughness that will enhance dissolution. In addition, I hypothesize that dissolution will result in a more spatially uniform distribution of erosion scales as compared to abrasion because chemical dissolution is the product of water running over the entire bed whereas abrasion is the end result of sediment particles impacting the bed in localized areas.

Through laboratory experiments, we actively eroded a flume bed made of plaster of paris (gypsum, $CaSO_4 \cdot 2H_2O$) with water and very fine gravel to observe the processes of dissolution and abrasion. Plaster of paris was used as a proxy for carbonate rock in these experiments due to its high solubility relative to carbonates and ability to be easily cast into a suitable size and shape. High resolution measurements of topography were made with a triangulating laser and 3-D scanner to quantify changes in the bed form as physical and chemical erosion occurred. The spatial and temporal evolution of erosion rates and surface roughness were quantified from topography. Electrical conductivity was measured throughout the experiments to infer rates of gypsum dissolution and link water chemistry with changes in physical bed topography.

I find that the spatial distributions of erosion are dependent on whether the bed topography has evolved due to dissolution or abrasion. The erosion distributions for both dissolution and abrasion are positively skewed with the most of the changes in bed topography being in contained areas of high erosion. However, across experiments, the erosion distributions for dissolution are closer to normal than the distributions for abrasion.

Table of Contents

List of Tables

List of Figures

Chapter 1: *Introduction and Methodology*

INTRODUCTION

Mechanical erosion processes, such as impact wear from transported bedload sediment, are typically seen as dominant in comparison to the chemical dissolution and erosion of rocks in river channels. However, in the case of relatively soluble rocks, such as carbonates and evaporites, dissolution could account for a significant role in erosion. Limestone surfaces are subject to transverse erosional features as a result of the mass transfer from dissolution, which appear as scallop marks; the form of erosional marks created by isolated defects is dependent on the duration of erosional processes and stability character of original defects (Allen et al., 1971). Carbonate surfaces develop the most diverse array, densest accumulation, and best-formed examples of bedforms as a result of dissolution (Richardson and Carling, 1971). Limestones develop a variety of solutional forms, chiefly solution pits and scallops, and these are bedforms that occur on a much smaller scale than most sculpted forms in other lithologies (Richardson and Carling, 1971). Covington et al., 2015 used data from 28 stream sites in various locations that were located on carbonate rocks or flowed onto carbonate rocks. Based on gaging station monitoring of water chemistry, they calculated that theoretical dissolution rates could range from 0.005 mm $year^{-1}$ to 4.85 mm $year^{-1}$ with the bulk of sites falling between 0 and 1 mm $year^{-1}$. It was also determined that chemical erosion can be expected to have the greatest effects relative to physical erosion where small catchments

flow from non-carbonate rocks onto carbonate rocks due to the water being the most chemically under saturated with respect to calcite.

A series of studies were conducted on carbonate terrains in central Israel to determine the effects of precipitation on chemical dissolution and the relative importance of chemical weathering as compared to mechanical processes. Although this thesis is laboratory-based and not linked to any particular field site, the findings of these studies assist in the linkage between flume observations and the comparative effects of chemical and physical erosion in natural settings. Ryb et al. (2015) found that erosion in this landscape is chiefly controlled by carbonate dissolution via precipitation on annual, decadal, and 10^4 year timescales. Similarities in HCO^{3-} concentrations in runoff, springs, and regional aquifer water indicated that chemical weathering focused on the bedrock surface as a result of solutional denudation (Ryb et al., 2014). Where climate was characterized by a significant rain shadow, erosion rates of bedrock outcrops differed from about 20 mm ka^{-1} in the wetter Mediterranean zone to 1-3 mm ka^{-1} in the hyper-arid zone. It was found that denudation rates of steep bedrock surfaces depend on hillslope gradient, suggesting that mechanical processes control overall hillslope erosion rates in the steeper landscape in the hyper-arid climate. The transition from chemically-dominated denudation to mechanically-dominated denudation in this landscape occurred between 100 and 200 mm of mean annual precipitation (which was established by the relation between denudation rate and hillslope gradient). In wetter climates, erosion from dissolution was more evenly distributed across the landscape and was relatively independent of local hillslope gradient, whereas for drier areas the denudation of

detachment-limited hillslopes had a strong relationship to local gradient (Ryb et al., 2014).

In the flume experiments conducted for this thesis, determining the distribution of erosion scales on the flume bed area may assist in decoupling dissolution and abrasion processes. Abrasion in open bedrock channels involves the wearing away of a surface from multiple impacts of sediment particles transported in fluid carried in suspension or as bedload or both. Each impact with sufficient energy breaks off a small part of the bedrock material, which in the case of coarse bedload, may be as much as a substantial chip of rock (Richardson and Carling, 1971). Chemical weathering directly removes rock over the entire surface via dissolution and indirectly physically weakens the rock (Richardson and Carling, 1971). As the effects of erosion occur over different surface areas for dissolution and abrasion, we expect that the processes may be able to be distinguished based on their distributions of cumulative erosion and the topography that gradually evolves from differing processes.

Through sediment transport, abrasion can contribute to landscape denudation where sediment impacts the river bed. Sediment can be drawn by gravity to topographic lows and results in further erosion of these topographic lows; however, increases in bedrock channel roughness amplitude are limited by the turbulent energy dissipated by form drag that will eventually result in flow only transporting the sediment load resulting in abrasion from alluvial cover (Johnson and Whipple, 2007). Additionally, through flume experiments of abrasion with gravel on a weak concrete “bedrock”, erosion rate increased linearly with sediment flux, bed roughness was enhanced due to sediment

dominantly traveling through topographic lows, and erosion was concentrated along these areas of increased bedload transport (Johnson and Whipple, 2010). This might create a positive feedback between the erosional features created by dissolution and the further mechanical weathering via abrasion.

Models and lab experiments on predicting partial alluvial cover in bedrock channels indicate that bed roughness is an important factor on both shear stresses and thresholds of sediment motion (Finnegan et al., 2007; Johnson and Whipple, 2007; Nelson and Seminara, 2011; Turowski et al., 2008). Johnson (2014) presented a model for surface roughness of an alluvial-bedrock bed that is dependent on the fraction of sediment cover. Shear stress has a positive relationship with surface roughness, which will result in increased transport capacity. However, thresholds of motion will also increase with surface roughness causing decreased transport capacity. Overall, changes in bed roughness can lead to varied cover responses. Roughness feedbacks indicated by the model show that partial alluvial cover can be in equilibrium with supply and cover-dependent transport capacity. Furthermore, the roughening of the channel increases the probability that moving sediment grains will come to rest in sheltered locations where local shear stresses are lower. Additionally, bed roughness will cause an increase in the friction angle for stationary grains on the bed, increasing grain resistance to motion (Kirchner et al., 1990). The denudational effects of abrasion on the bed topography might be partially predicted by the factors of alluvial cover and bed roughness.

Flume experiments have been conducted on plaster of paris ($CaSO_4 \cdot 2H_2O$) beds to produce dissolution patterns from the interaction of a soluble surface and adjacent

turbulent flow. Plaster of paris is considered a viable proxy for carbonate bedrock due to its high solubility in comparison to carbonates and ability to be molded into a controllable size and shape. The solubility of gypsum in pure water at 20˚C is 2.5 g/L or 14.7 mM/L, roughly three orders of magnitude greater than the solubility of $CaCO_3$ (1.5 mg/L) (Klimchouk, 1996). In addition, the effective dissolution rates of gypsum are governed by mixed kinetics, where the rate constants of dissolution at the surface and the transport constant of molecular diffusion of dissolved material are similar. Dissolution batch experiments on pure synthetic gypsum indicate a linear rate law up to equilibrium with dissolution inhibition present in natural samples close to equilibrium, a phenomenon that is also known for calcite materials (Jeschke et al, 2000).

In a flume based study on the effect of surface roughness on mass transfer of plaster of paris, it was concluded that Ca^{2+} was the only major cation to increase in concentration throughout the experiments and gypsum dissolution was measured in their experiments as an increase in calcium ions in freshwater recirculating over the experimental surface (Baird and Atkinson, 1997). Gypsum dissolution can thereby be approximated through flume experiments by measuring electrical conductivity and the equivalent total dissolved solids concentration.

While flume based studies have been previously done separately on the effects of dissolution (Allen, 1966, 1971; Baird and Atkinson, 1997; Goodchild and Ford, 1971) and abrasion (Johnson and Whipple, 2007, 2010; Kirchner et al., 1990; Sklar and Dietrich, 2001) as independent processes on bedrock, to my knowledge there have not yet been experimental studies integrating both observations to link chemical and physical

erosion and understand possible feedbacks on each other. Also, past experiments have focused on re-creating erosional features that would be the result of chemical weathering in karst settings (Allen et al., 1971), but limited work has been done to study the magnitude and variation of dissolution rates of streams in carbonate landscapes.

This set of flume experiments seeks to determine how the processes of dissolution and abrasion are actively eroding a plaster of paris bed. We attempt to quantify changes in the bed form as physical and chemical erosion proceed to estimate surface roughness and distinguish erosion distributions between dissolution and abrasion. I hypothesize that dissolution and abrasion will cause subsequent increases in bed roughness that will enhance dissolution processes. In addition, spatial distributions of erosion scales across the bed are expected to be closer to a normal distribution for dissolution as compared to abrasion.

METHODOLOGY

The experimental flume used for this project was 4m long by 0.1m wide. Data were collected over a working length of 2.4 m in order to minimize inlet and outlet effects. The flume was constructed and designed to geometrically scale to natural channels (Johnson et al., 2015). This flume design allows for control of the following variables: water discharge, water temperature, upstream sediment flux and grain size distribution, and initial bed slope. The 5% initial bed slope was established to simulate a typical gradient of a steep mountainous stream. An auger-style sediment feeder was placed at the upstream side of the flume and fed sediment at a controllable rate to the channel bed. Parameters measured in the flume during each experimental time step

included: channel bed elevation (along the flume centerline), bed topography, average flow depth, flow rate, sediment transport rates, sediment spatial distribution, water electrical conductivity, and water temperature. Electrical conductivity was measured throughout the experiments to infer rates of gypsum dissolution and link water chemistry with changes in physical bed topography. The sediment grain size was a fine gravel (D16=2.0mm; D50=2.4mm; D84=2.8mm) (particle Re = 282) and was chosen so that flow around grains would be hydraulically rough, consistent with flow around gravel in typical gravel-bed and bedrock rivers (Parker et al., 1991; Parker et al., 2007). The particle Reynold's number was calculated by the following equation:

$$Re_p = \frac{U_p D}{v} \quad [1]$$

where U_p is the characteristic particle (shear) velocity, D is the grain diameter, and v is the kinematic viscosity, which is given by the dynamic viscosity (μ) of water at 30 degrees Celsius (0.8×10^{-6} m^2/s) divided by the fluid density (ρ_w) (1000 kg/m^3). U_p is calculated as:

$$U_p = \sqrt{\frac{\tau}{\rho_w}} \quad [2]$$

where τ is the shear stress. Shear stress is calculated by the following equation:

$$\tau = \rho_w g h \quad [3]$$

where g is the acceleration due to gravity (9.81 m/s^2) and h is the average water depth in meters (0.018 m).

Instrumentation was installed on the flume to measure the aforementioned parameters. A motorized cart that ran along the top of the flume was equipped with a Keyence triangulating laser and a Massa ultrasonic transducer to record channel bed elevations and water surface elevations, respectively, along the flume centerline. Topographic roughness was calculated using the standard deviation of the de-trended bed elevations over the working length of the flume (Finnegan et al., 2007; Johnson and Whipple, 2007). Water depth was calculated as the difference between the water surface and bed surface elevations. A string transducer recorded the location of the cart along the working length of the flume. An Omega magnetic flow meter was installed on the water discharge pipe at the upstream end to accurately record flow rates. A basket at the downstream end of the flume collected transported sediment throughout each experiment. Photographs were taken from flume overhead cameras during experiments involving sediment feed to determine the spatial distribution and probability of grains being in a given location, although these data are not included in the analysis at present. An HDI Advance white-light 3-D scanner was mounted above the flume to take high-resolution measurement of bed topography (1 mm measurement spacing with a vertical accuracy of 0.3 mm at two standard deviations). In the tank at the downstream end of the flume, an Omega conductivity/temperature meter measured electrical conductivity (from which total dissolved solids concentration can be inferred) continuously as the experiments proceeded. An aquarium heater was used to maintain water temperature between 30-31 degrees Celsius to accelerate the gypsum dissolution rate. The temperature chosen was

based on Thompson and Glenn, 1994, which fit fraction of gypsum material dissolved versus temperature and water velocity to the following equation:

$$\frac{\Delta W}{W_i} = 1 - \left[1 - 0.71\left(\frac{A_i}{W_i}\right)\left(\frac{T}{T_{ref}}\right)\left(\frac{\mu}{\mu_{ref}}\right) x\, V^{0.8}\Delta C_{25}\theta\right]^3 \quad [4]$$

where $\frac{\Delta W}{W_i}$ is the fraction of gypsum material dissolved, A_i is the initial bed area, W_i is the initial weight, T is the temperature, T_{ref} is 25 degrees Celsius, μ_{ref} is the dynamic viscosity of pure water at 25 degrees Celsius (or 889 x 10^{-4} Pa*s^{-1}), μ is the dynamic viscosity at the experimental temperature, ΔC_{25} is the concentration difference computed at 25 degrees Celsius, θ is the time in days, and V is the water velocity. The dynamic viscosity at the experimental temperature was determined by the following equation:

$\mu(T) = 2.414\ x\ 10^{-5}\ x\ 10^{\frac{247.8}{(T-140)}}$ for temperatures between 273˚to 643˚Kelvin and μ has units of $Pa\ \cdot s$. Equation 4 shows that gypsum dissolution is sensitive to temperature as the temperature term in the equation is cubed. By increasing the temperature from 25˚C to 30˚C, the fraction of gypsum material dissolved increases by 20%. James (1992) presented data for plaster of paris dissolution showing the dependence of solubility of gypsum in pure water on temperature shown in Figure 1.

Experiments began with a relatively smooth plaster of paris bed that was poured into the base of the entire length of the flume and allowed to set. The plaster was prepared by mixing No. 1 pottery plaster (US Gypsum) with water. This product was chosen because it was used to study dissolution in a previous experimental analysis of the

effects of nonlocal turbulence on the mass transfer of dissolved species to reef corals (Falter et al., 2007). In order to pour a bed that was 5 cm in thickness, 19.9kg of plaster were mixed with 13.9kg of water. Some surface undulations were present in the initial bed as the plaster did not level itself following the pour. Bed topography subsequently evolved due to erosion, as shown in the 3-D scans in Figure 2. Table 1 shows the conditions used in the sequence of experimental time steps.

During solely dissolution experiments, water discharge was turned on at an average constant rate of 4.2×10^{-4} m^3/s (0.42 liters/s) and allowed to flow over the bed for 4hr and 16hr time step durations. While flow was running, water surface elevations were collected using the ultrasonic transducer. At the end of the time step, discharge was stopped and the bed topography was measured using the Keyence triangulating laser and 3-D scanner. The water was allowed to recirculate through the flume during time steps and water temperature and electrical conductivity were measured using a meter in the downstream tank. As these experiments were somewhat exploratory, the tank water was changed for new tap water under saturated with respect to gypsum at different time step durations to determine the optimal times for erosion by dissolution.

During experiments with the addition of sediment causing abrasion, sediment feed was introduced to the channel at a rate of 10 g/sec. For these experiments, fine gravel was fed into the upstream end of the flume by the sediment feeder. This sediment feed rate was selected to allow for sufficient sediment to impact the bed and induce denudation. Additionally, the sediment feed rate was chosen to have sufficiently limited alluvial cover over the channel bed so the bed would likely be abraded. Each sediment feed time step

lasted for a duration of 90 or 180 minutes. Sediment was collected in a basket in the downstream tank and weighed after each time step. All previously described measurements (i.e. bed and water elevations) were taken at the 90 or 180-minute intervals in conjunction with the sediment feed.

Hydraulic Roughness

The "total" hydraulic friction factor is calculated using the Darcy-Weisbach equation for friction factor f_{total} as:

$$f_{total} = \frac{8gR_hS}{v^2} \quad [5]$$

where R_h is hydraulic radius (cross-sectional area/wetted perimeter) and v is average flow velocity. R_h was calculated from the average flow depth and flume width (Comiti et al., 2009). v was calculated for each time step from the measured flow depth, flume width, and discharge. S is the average bed slope. Hydraulic friction factors are compared to bed roughness in the results section below.

Dissolution Rates

The dissolution of gypsum is mass-transfer limited (Barton and Wilde 1971) and can be described as a first-order rate reaction with respect to the concentration gradient through the boundary layer (Baird and Atkinson, 1997) :

$$m_s = S(C_b - C_w) \quad [6]$$

where C_w (mol m^{-3}) is the concentration of gypsum at the interface between the bed and water, C_b (mol m^{-3}) is the gypsum concentration in the water beyond the diffusive

boundary layer and S (m s^{-1}) is a boundary-layer mass-transfer coefficient. S can be divided into two variables, the dimensionless Stanton number (St_m) and the water velocity (U_b).

$$m_s = St_m U_b (C_b - C_w) \quad [7]$$

St_m corresponds to the solute-uptake rate to the bed divided by the advection of the solute over the bed bottom and is an indicator of uptake performance of a known area of the bed. St_m is generally determined under experimental conditions where C_w is assumed to be negligible in comparison to C_b.

Similar to equation 6, dissolution rates are dependent on boundary layer conditions and the concentration gradients across it as described in the following equation:

$$\frac{dC}{dT} = \left(\frac{KA}{V}\right)(C_s - C)^n \quad [8]$$

Where dC/dT is the rate of change of concentration in a volume V of solution with a bulk concentration C (determined based on the total dissolved solids concentration), C_s is the solubility of the dissolved substance (established based on measured experimental temperature and fitting data to the curve presented in Figure 1), A is the surface area, n is the order of the kinetic equation, and K is a rate constant depending on boundary layer conditions, mineral properties, and surface roughness (Klimchouk, 1996). At the transition from laminar to turbulent flow over calcite, an increase by a factor of ten is reported to occur for the rate constant, K, and a similar increase is expected for gypsum

as postulated by James (1992). The turbulence created by large scale roughness controls dissolution rates by setting the thickness of the concentration boundary layer (Hearn et al., 2001).

As both calcite and gypsum dissolution follow first-order kinetic equations, if Equation 8 is integrated, the result is:

$$Ln\left[\frac{C_s}{C_s - C}\right] = \frac{KAt}{V} \quad [9]$$

And hence a graph of:

$$Ln\left[\frac{C_s}{C_s - C}\right] \; vs. \; time \quad [10]$$

for first-order kinetics should take the form of a straight line through the graphical origin with slope KA/V. Additionally, fitting an exponential function to data of conductivity versus time elapsed since water change results in an equation of the form:

$$f(x) = ae^{-bx} + c \quad [11]$$

where a, b, and c are constants and c is equivalent to the asymptotic value at which saturation state approaches 100%.

I designed the experimental procedure in order to record observations and relationships between evolving erosion rate, erosion patterns, channel topography and surface roughness, sediment supply, and water chemistry. In accordance with having consistent average flow rates, water temperature, and sediment flux (in experiments involving abrasion), the experiments can be reasonably compared to one another in order

to discern trends and effects from changes in electrical conductivity, bed roughness, hydraulic roughness, and bed topography. This experimental setup provides observations of channel dynamics as a result of dissolution and abrasion processes.

A summarized sequence of time steps conducted (as detailed in Table 1) is as follows: 60 hours of dissolution were conducted prior to beginning experiments incorporating abrasion. The abrasion experiments occurred after the water circulating the flume had sufficient time to reach saturation with respect to gypsum. Six abrasion time steps were conducted directly following the 60 hours of dissolution. In addition, three time steps each of alternating dissolution and abrasion were conducted. The duration of dissolution and abrasion intervals were 16hr and 90min respectively and maintained the same sediment feed rate (10 g/s) for periods of abrasion. The first of these three experiments started with fresh tap water in the downstream tank that was allowed to come into saturation with respect to gypsum. The water was recirculated through the flume throughout the three alternating time steps. Also, one time step of 16hr of dissolution followed by 180min of abrasion was undertaken. Measurements with instrumentation were taken after 4 and 16 cumulative hours of dissolution and after 3hr of abrasion. The dissolution and abrasion were followed by one additional 16hr dissolution period with measurements taken at the same intervals as the first two dissolution time steps.

Chapter 2: *Results*

Three sets of experiments were run (with different durations of dissolution and abrasion time steps), each made up of two parts: part (1) was composed of running water over the bed until the change in conductivity reached relatively steady state, the flume water was saturated with respect to gypsum, and limited additional dissolution was occurring and part (2) added sediment feed into the channel composed of fine gravel (D50=2.4mm) (see Table 1). These two experimental parts showed distinct differences in data with regard to change in conductivity readings and distribution of erosion scales and bed roughness on the flume bed.

Electrical Conductivity

Changes in conductivity reached relatively steady state after 16hr of dissolution from recirculating the same tap water over the bed throughout the duration of the experiment. Figure 3 shows plots of conductivity and total dissolved solids versus elapsed time (in hours) for 16hr of dissolution followed by 3hr of abrasion (experiments 19 and 20 respectively). The elapsed time extends past 19hr because during the abrasion time step, the downstream basket collecting sediment could only hold a certain amount of sediment before having to be cleared. The flume was allowed to keep circulating water during these clearing periods. After 16hr the conductivity continues to increase at the end of the dissolution period and during the abrasion time step but at a very slow rate. The slight decrease in conductivity at the beginning of the abrasion time step is due to the addition of water to the downstream tank to return it to the same starting water level as the dissolution time step to maintain close to uniform discharge between time steps.

The conversion between conductivity and total dissolved solids for $CaSO_4$ is 1 ppm TDS = 1 µs/cm. Total dissolved-solids values in milligrams per liter should be typically 0.55 to 0.75 times the specific conductance in micromhos per centimeter (equivalent to microsiemens per centimeter) for waters of ordinary composition, up to dissolved-solids concentrations as high as a few thousand milligrams per liter. Waters saturated with respect to gypsum may have factors as high as 1.0 (Hem, 1985) and we use this conversion factor in this study.

Plots of conductivity and total dissolved solids versus elapsed time since water change are shown in Figure 4 for the period between time step 1 and 2. The conductivity increased steadily from 0.3 to 1.65 mS/cm during four hours of dissolution on the initial flume bed.

Between time steps 13 and 14, water was run over the bed for 16hrs inducing dissolution. Conductivity increased modestly from 2.62 to 2.66 mS/cm (see Figure 5) as the water recirculating the flume had already been saturated with respect to gypsum as previous dissolution and abrasion time steps (elapsing 18.65hrs) had already been conducted. Similarly during time step 15, during which 90min of abrasion occurred, conductivity increased slightly from 2.66 to 2.67 mS/cm. During time step 17, conductivity showed a small increase from 2.70 to 2.74 mS/cm.

During time step 22, 4 hrs of dissolution occurred with conductivity increasing relatively rapidly due to the unsaturated state of the flume water with respect to gypsum. As shown in Figure 6, conductivity increased from 0.3 to 1.8 mS/cm between time steps

20 and 22. Between time steps 22 and 23, conductivity increased to a value of 2.5 mS/cm before reaching near steady-state conductivity.

The relationship between average conductivity in a time step and erosion rate are shown in Figure 7. Erosion rates were calculated by averaging the change in bed elevation over the duration of the time step. Overall, at high average conductivities (2.6-2.7 mS/cm) (where the water is relatively saturated with respect to gypsum), there tends to be lower erosion rates in the time step. When average conductivities are lower (1.1-1.2 mS/cm) and the water has not yet come to saturation with respect to gypsum, the erosion rates are higher.

Bed Roughness

Bed roughness is quantified by determining the standard deviation of bed topography from mean bed elevation as described in the methods. Figure 8 shows bed roughness values throughout the entire experimental period with selected time steps labeled. Bed roughness increased during both dissolution and abrasion time intervals. From the processed data available, bed roughness appeared to change rapidly in dissolution experiments where the flume water was unsaturated with respect to gypsum and then bed roughness increases slowed when the water was closer to saturated. In addition, a plot of hydraulic roughness (total friction factor) versus bed roughness (Figure 9) for time steps 13 through 22 indicates a positive relationship between the two variables. As bed roughness increases as a result of dissolution and abrasion, hydraulic roughness similarly increases.

Distribution of Erosion Scales

After aligning the 3-D scan images, it was found that the best image alignment existed for the center of the flume bed, which spanned 129cm. Therefore, erosion rates were calculated from the four center images by differencing the changes in bed elevation between time steps. See Figures 10 and 11 for examples of an erosion difference maps. Qualitatively the erosion maps show the areas of greatest erosion. Based on the color bar for the erosion maps, the areas of highest erosion are red (up to 2mm); however greater erosion can exist locally. The uncertainty of cumulative erosion was determined by the difference in erosion between repeated scans in the same bed locations (± 0.3 mm at the 95% confidence interval).

The spatial distributions of erosion scales for dissolution and abrasion appear different (see Figure 10 for dissolution time steps and Figure 11 for abrasion time steps). For all dissolution time steps, it was found that the distribution of erosion scales across the bed was relatively uniform and laterally extensive (Figure 10). The best examples are seen for the difference maps between time steps 17 and 19 and time steps 20 and 22. In examining time steps involving abrasion (see Figure 11), between time steps 14 and 15 (after 90min of abrasion), the erosion was largely concentrated in the center of the flume bed. For time steps 19 and 20 (after 180min of abrasion), the highest erosion rates (up to 2 mm) were still found in the center of the bed. However, there was a greater lateral distribution of erosion for the longer duration time steps than the shorter duration time steps. In qualitatively contrasting the distribution of erosion between dissolution and

abrasion, erosion resulting from abrasion is more focused in localized areas of the bed, while erosion from dissolution is more evenly distributed across the bed.

Figures 12 and 13 show the distribution of erosion scales and associated normal probability plot across the same bed area for four dissolution time steps of different durations and post water change times. Figure 12 is a histogram with the normalized frequency of occurrence at a peak of 1. In Figure 13, the same data have been fit to a normal distribution and translated to a normal probability plot, which displays how much the data deviate from a normal distribution by comparing the data curve to a straight line (which represents a perfect Gaussian distribution fit to the data between cumulative probabilities of 0.25 and 0.75). Figures 14 through 17 display distributions and normal probability plots of erosion for abrasion and dissolution time steps. Figures 18 and 19 show the distribution of erosion scales and normal probability plot for abrasion time steps of different durations. The median erosion values and interquartile range values for the processed time steps are shown in Table 2.

Chapter 3: *Discussion and Conclusions*

DISCUSSION

The experiments were designed to observe and quantify bedrock erosion due to the processes of abrasion and dissolution. Whereas abrasion results in physical erosion from sediment impacting the bed in localized areas of increased bedload transport, dissolution is the product of mass transfer distributed over the entire area where water is running over the bed. Chemical and physical erosion caused not only decreases in bed elevation but also increases in bed roughness as experiments proceed. We interpret the distinction between the distribution of erosion scales for dissolution and abrasion and the relationship between increased bed roughness and mass transfer rate.

Distribution of Erosion Scales in Dissolution Time Steps

Little to no erosion occurred during the dissolution interval between time steps 13 and 14 (after approximately 35 hours of water running over the bed surface) because the flume water was near saturation with respect to gypsum. As Figures 12 and 13 indicate, the measured statistical distribution of “erosion” in this time interval is almost identical to the distribution of measurement uncertainty derived from repeat scans of the bed during the same time step (t14). Therefore this time interval serves as a comparison of uncertainty in cumulative erosion to other dissolution time steps where greater erosion was occurring.

Distributions for the erosion between dissolution time steps 17 and 19 (t17-t19) and time steps 20 and 22(t20-t22) (see Figure 10 for the erosion difference maps) are similar in the magnitude of deviation from the normal distribution (Figures 12 and 13).

The difference in the ranges of the majority of erosion varied for the two distributions due to the duration of the time steps and corresponding differences in water conductivity (Figure 7). The greater interquartile range and higher median are expected for t17-t19 as it is a longer duration time step (16 hours) than t20-t22 (4 hours) and more dissolution will occur as water is running for a longer period over the bed (Table 2). Both distributions are right-skewed indicating that higher cumulative erosion occurred on localized parts of the bed, possibly in areas where bed roughness was greater and dissolution was enhanced.

For erosion between time steps 1 and 2 (t01-t02), the distribution was also right-skewed but somewhat less so than t17-t19 and t20-t22 (Figures 12 and 13). t17-t19 and t20-t22 occurred after multiple time steps of dissolution and abrasion had been induced on the bed. This caused greater bed roughness which exposed more bed surface area to potentially erode. t01-t02 represents the initial period of dissolution (4 hours) on a less rough bed with limited topographic variation. As not enough time between time step 1 and time step 2 had elapsed for well distributed bed roughness to develop, the erosion distribution was more close to normal than t17-t19 and t20-t22. However, Figure 10 qualitatively indicates local areas of high dissolution associated with local surface topography.

Between time steps 20 and 22, which was the change following 4hrs of dissolution (conducted after other dissolution and abrasion had already been induced on the bed), the bed roughness was significantly increased as compared to the period between time steps 1 and 2 (see Figure 8) and so cumulative erosion was higher overall

than the difference between time steps 1 and 2 (Figure 10). I find that significantly higher dissolution rates when the bed is rougher (t20-t22) compared to smoother (t01-t02) (see Table 2) for approximately the same change in fluid conductivity (see Figures 4 and 6 (first 4 hours)). Therefore, the data show that both surface roughness and water chemistry influence dissolution rates, consistent with previous work (Baird and Atkinson, 1997; Blumberg and Curl, 1974; James, 1992).

Comparing Dissolution and Abrasion Distribution of Erosion Scales

Overall, dissolution exhibits closer to normal distributions of erosion than abrasion, although both processes show positively skewed distributions. The stronger normal distribution for dissolution is attributed to the fact that water is running over the entire bed surface during time steps. I do not have measurements of turbulence in the flume, but there were undoubtedly spatial variations in turbulent intensity due to local bed topography that influenced local dissolution rates. Nonetheless, the entire flow was of course turbulent, and the entire bed surface area eroded by dissolution to some degree. In contrast for abrasion, the erosion is caused by independent sediment particles impacting the bed in localized areas of increased bedload transport. Based on the 3-D scan images showing the areas of greatest cumulative erosion, it appears qualitatively that the sediment is preferentially impacting the center of the flume bed where topographic lows have developed and that the upstream-facing surfaces have a greater probability of impact (see Figure 11). It is also apparent from overhead photos taken of the flume during abrasion time steps that the majority of sediment is being transported along the center of the flume bed (see Figure 20), which may be an effect of the limited flume

width. For this reason, I interpret that distributions of abrasion erosion will be further from a normal distribution than dissolution erosion time steps (Figures 15 and 17).

Comparing Abrasion Distribution of Erosion Scales

In comparing two abrasion time steps, 90min of abrasion (t14-t15) and 180min of abrasion (t19-t20), it was found that both time steps exhibited right-skewed distributions (Figures 18 and 19). For the longer (180min) time step duration, the bed had increased potential for spatially more of the bed to be impacted by sediment. During the shorter (90min) time step, the bed is incised mainly in the center of the bed where topographic lows have developed and focus abrasion in these areas of increased bedload transport. Abrasion is still centered on the middle of the bed during the longer time step, but the greater duration allows for more erosion to occur away from the center of the channel. These results are confirmed quantitatively by the higher cumulative erosion for t19-t20 (0.4015 mm) as compared to t14-t15 (0.2357 mm).

Scaling Gypsum and Calcite Dissolution Kinetics

The dissolution of gypsum and calcite are both first-order reactions (Klimchouk, 1996). Based on experimental data between time steps 7 and 8 and between time steps 20 and 22 (Figures 21 and 22), the flow time at which the solution approaches 90% of saturation is relatively short duration (approximately 8.6hrs); the rate of dissolution decreases by several orders of magnitude above this limit. In addition, the first-order kinetics of gypsum dissolution are displayed through the primarily linear relationship

between $Ln\left[\frac{C_s}{C_s-C}\right]$ and time (Equation 10) between dissolution time steps 7 and 8 (Figure 23) and time steps 20 and 22 (Figure 24).

CONCLUSIONS

The experiments described herein aim to determine the effects that dissolution and abrasion have on bed topography and channel roughness. I find that the spatial scales of erosion vary based on whether the bed topography has been altered by chemical or physical erosion. The erosion distributions for both dissolution and abrasion are right skewed with the most of the changes in bed topography being focused denudation in limited areas. However, throughout experiments, the erosion distributions for dissolution are more normal than the distributions for abrasion. Erosion distribution differences can be attributed to dissolution resulting from water running over the entire flume bed, in contrast to abrasion which occurs in localized areas where sediment impacts the bed. The conductivity data shows that the dissolution of gypsum in these experiments conforms to a first order reaction, where the data fits to an exponential decay curve with rapid increases initially corresponding to prompt dissolution when the water is far from saturation with a transition to much slower dissolution rates later. Additionally, the first order kinetics of gypsum dissolution are apparent from the linear relationship of plots of $Ln\left[\frac{C_s}{C_s-C}\right]\ against\ t$ for dissolution time steps. Gypsum dissolution rates are expected to increase in conjunction with bed roughness.

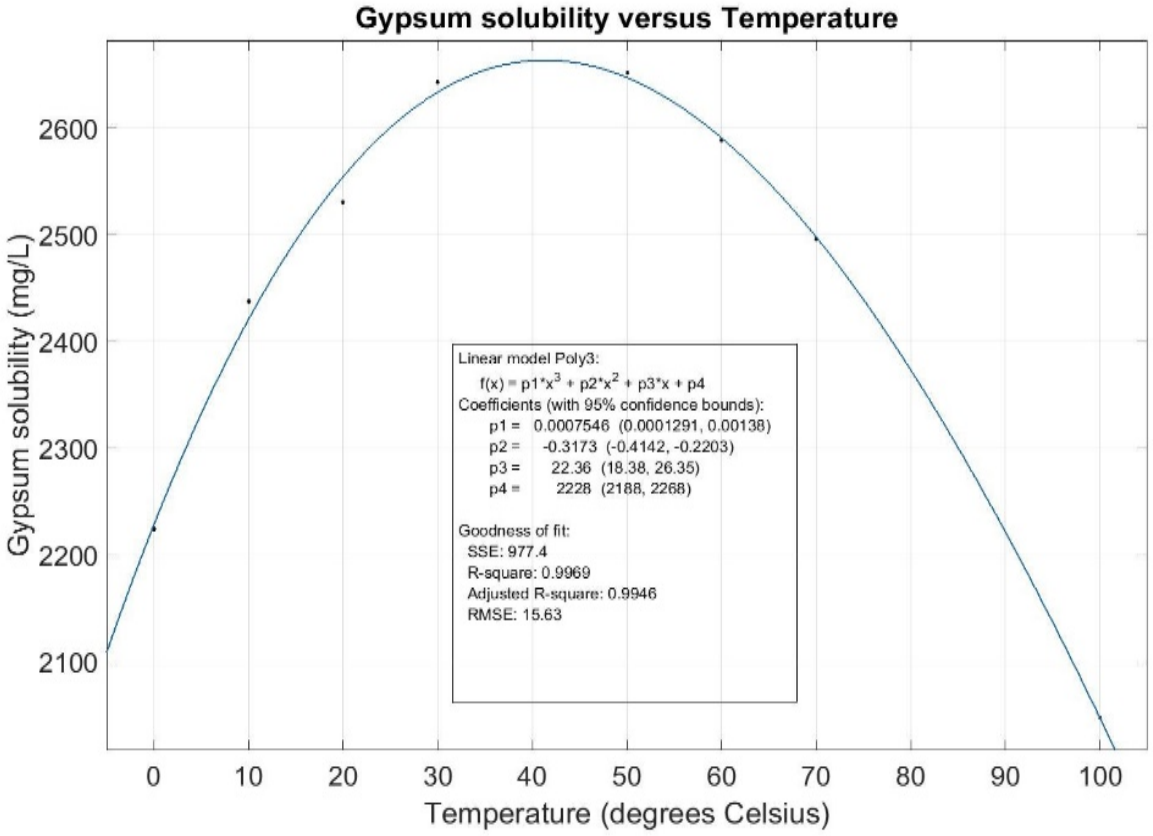

Figure 1: Plot of gypsum solubility (mg/L) versus temperature (degrees Celsius) based on data from James (1992).

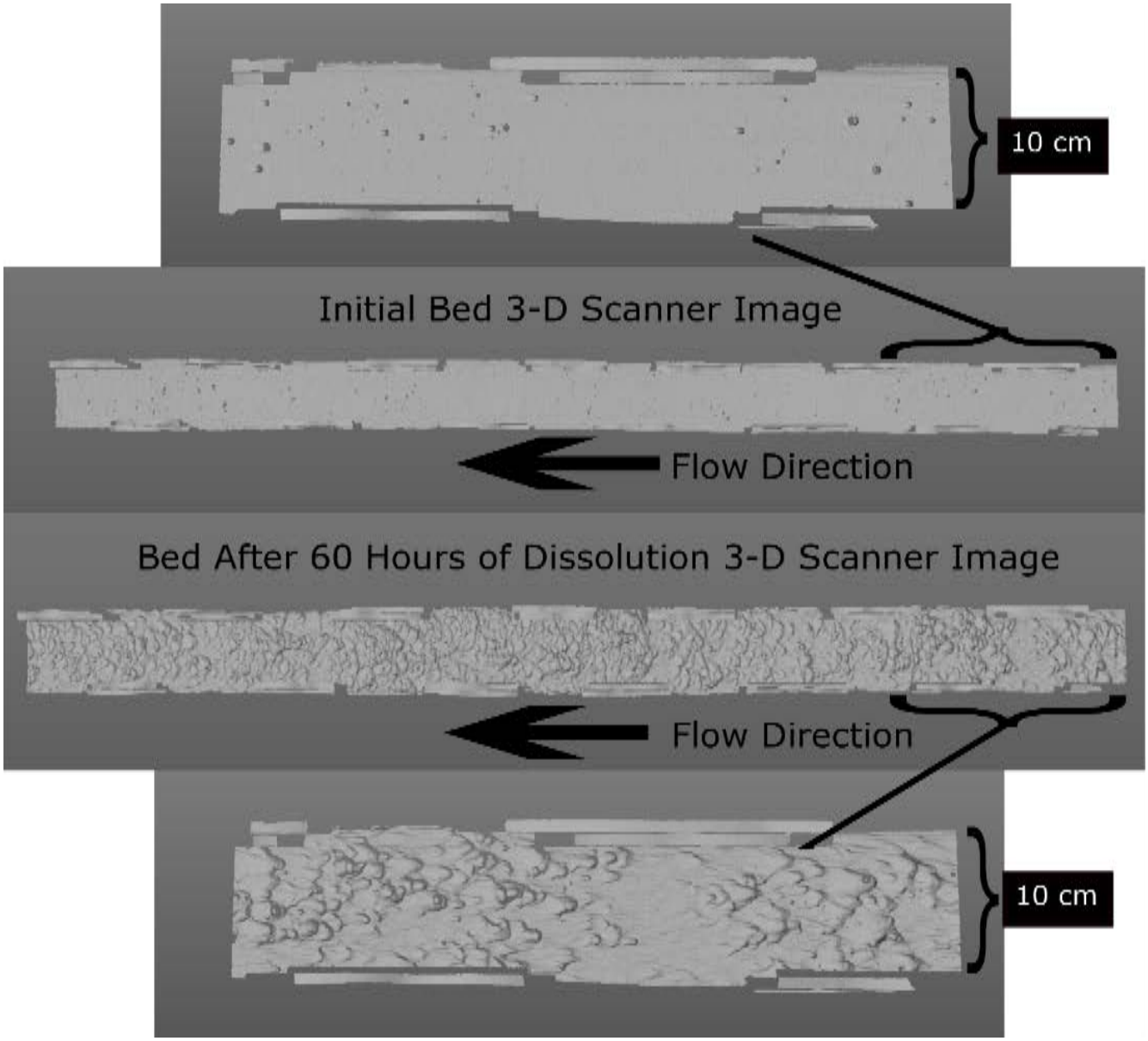

Figure 2: Images generated by 3-D scanner of plaster of paris flume bed at the beginning of experiment and following 60 hours of dissolution with water running over bed.

Experimental Time Step	**Time (Hours)**	**Time (hours)**	**Experiment Type**
	hours since tank water change	*duration of dissolution/abrasion*	
1	0	0	Initial Bed
2	4	4	Dissolution
3	0	See previous row	See previous row
4	4	4	Dissolution
5	16	16	Dissolution
6	0	See previous row	See previous row
7	4	4	Dissolution
8	16	16	Dissolution
9	0	See previous row	See previous row
10	9	9	Abrasion
11	0	0	See previous row
12	16	16	Dissolution
13	18.65	1.5	Abrasion
14	34.65	16	Dissolution
15	37	1.5	Abrasion
16	53	16	Dissolution
17	55.8	1.5	Abrasion
18	0	See previous row	See previous row
19	16	16	Dissolution
20	20.92	3	Abrasion
21	0	See previous row	See previous row
22	4	4	Dissolution
23	16	16	Dissolution

Table 1: Experimental time steps with hours since tank water change, duration of dissolution or abrasion, and experimental type (dissolution or abrasion).

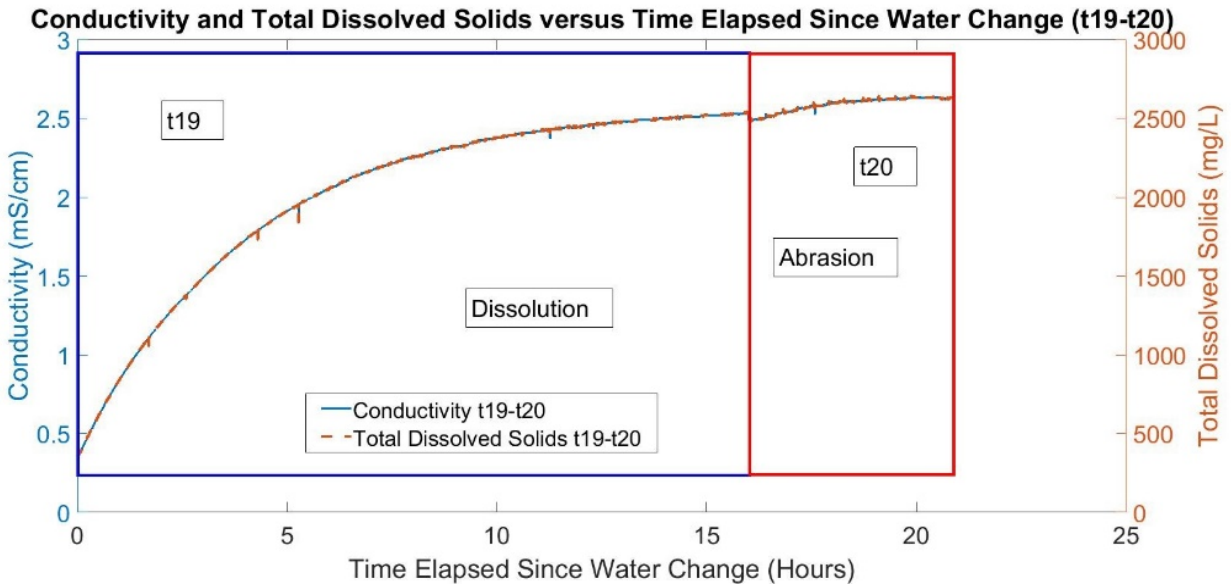

Figure 3: Plots of conductivity (mS/cm) and total dissolved solids (mg/L) versus elapsed time (hours) for time steps 19 and 20 (16hr dissolution followed by 3hr abrasion).

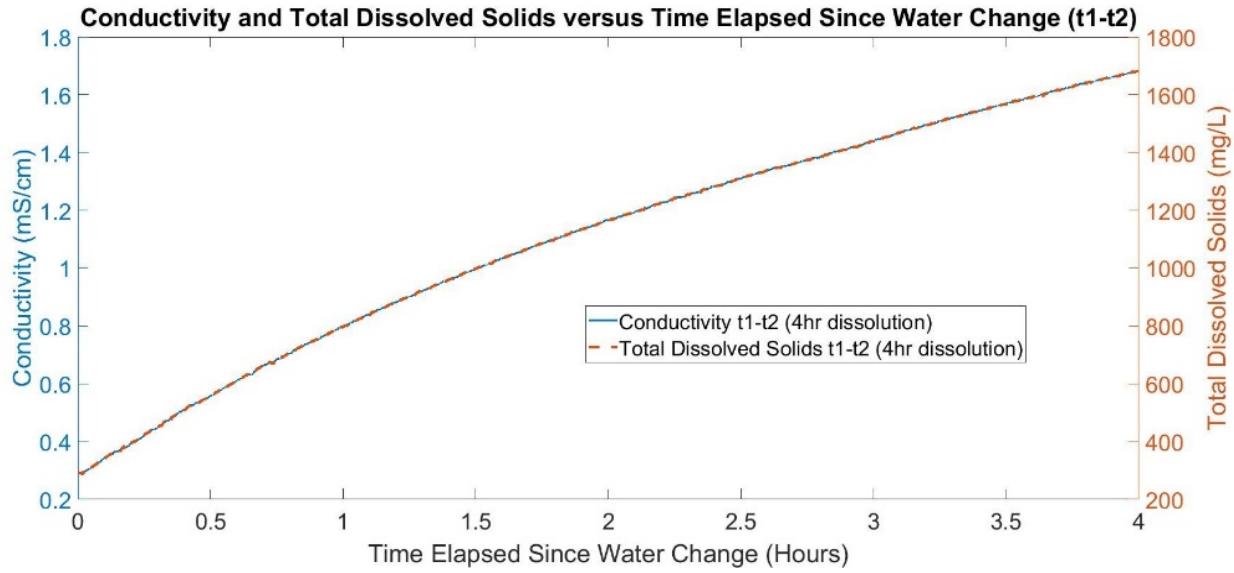

Figure 4: Plots of conductivity (mS/cm) and total dissolved solids (mg/L) versus elapsed time (hours) for time steps 1 and 2 (4 hours of dissolution on initial bed).

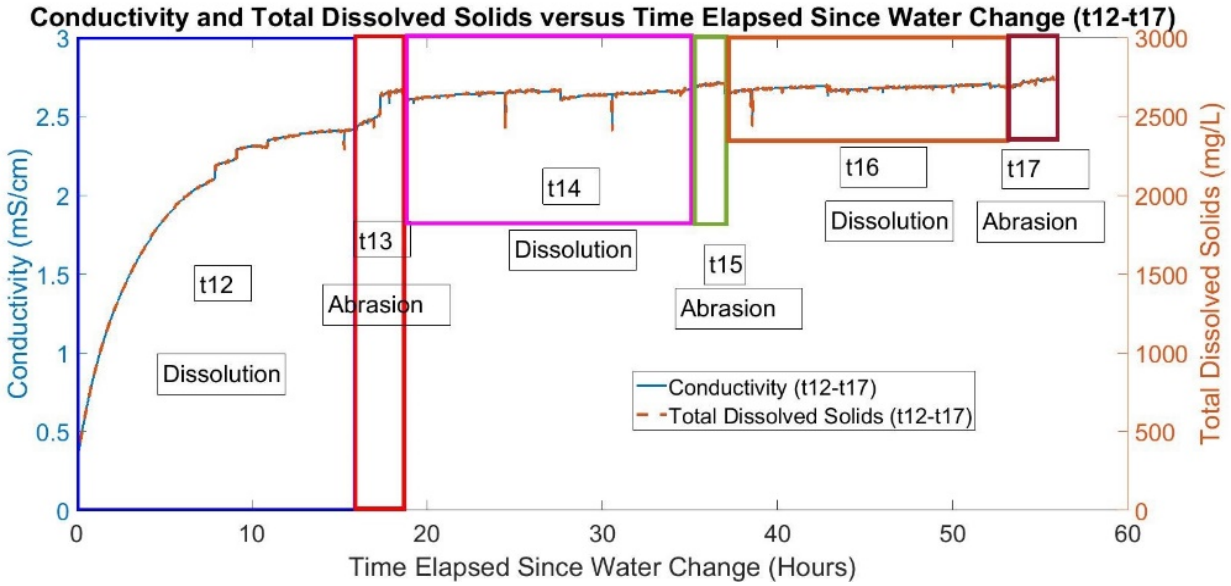

Figure 5: Plots of conductivity (mS/cm) and total dissolved solids (mg/L) versus elapsed time (hours) for time steps 12 through 17 (three sets of alternating time steps of 16 hours of dissolution and 90 minutes of abrasion).

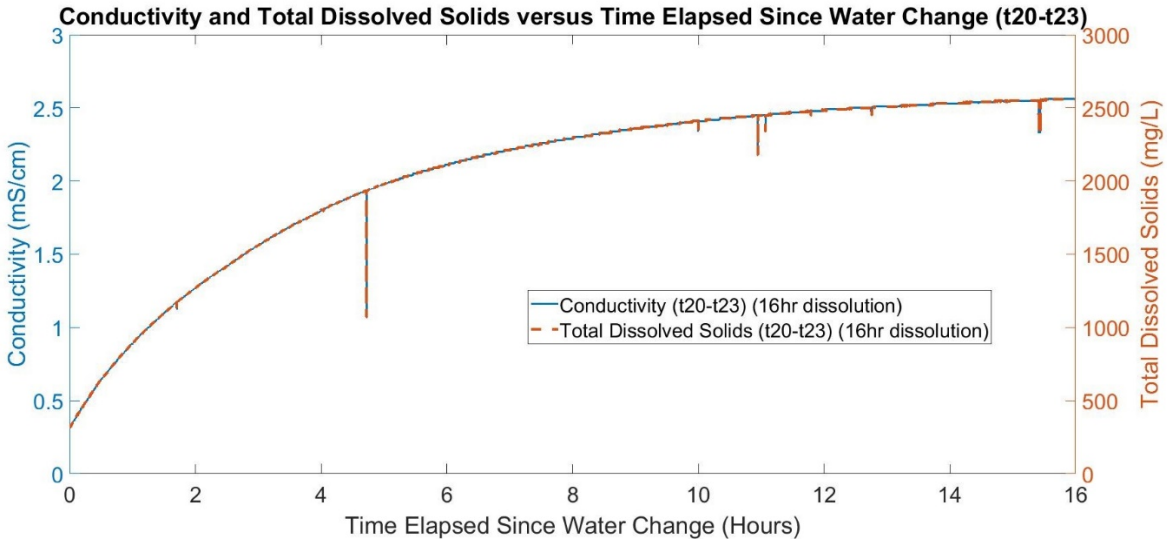

Figure 6: Plots of conductivity (mS/cm) and total dissolved solids (mg/L) versus elapsed time (hours) for time steps 20 through 23 (16hr dissolution).

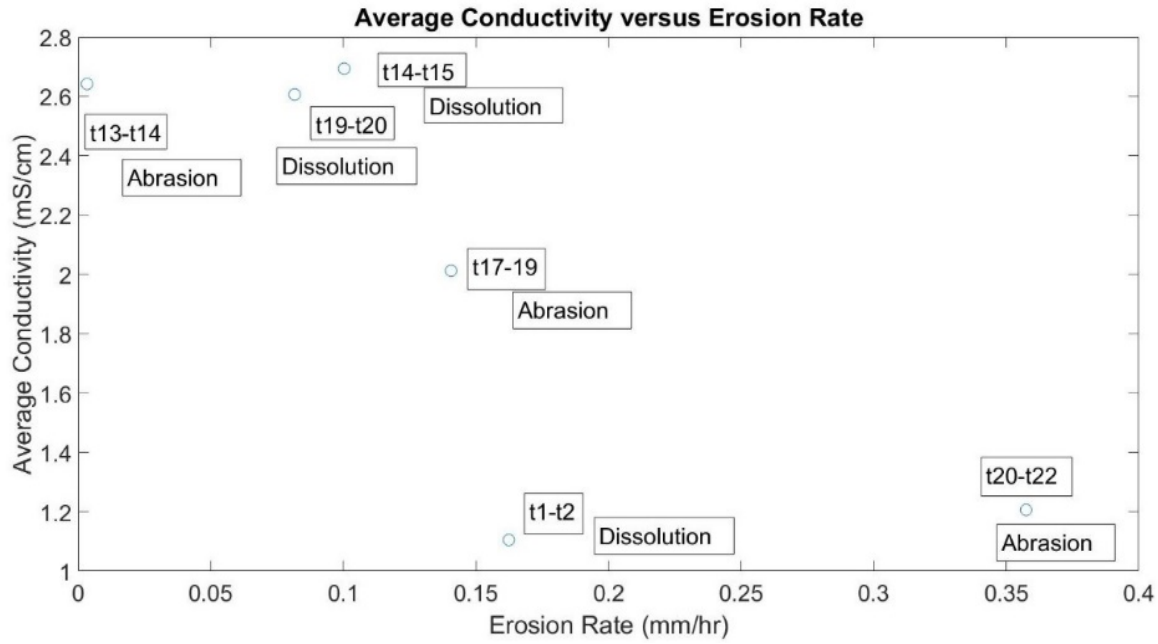

Figure 7: Plot of average conductivity (mS/cm) versus erosion rate (mm/hr) for selected time steps.

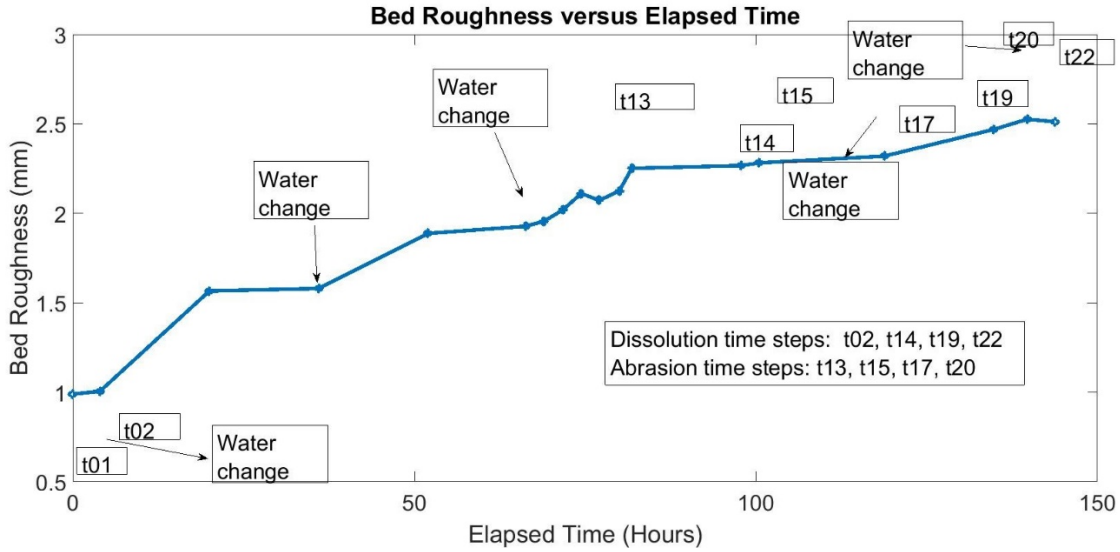

Figure 8: Plot of bed roughness (mm) versus elapsed time (hours).

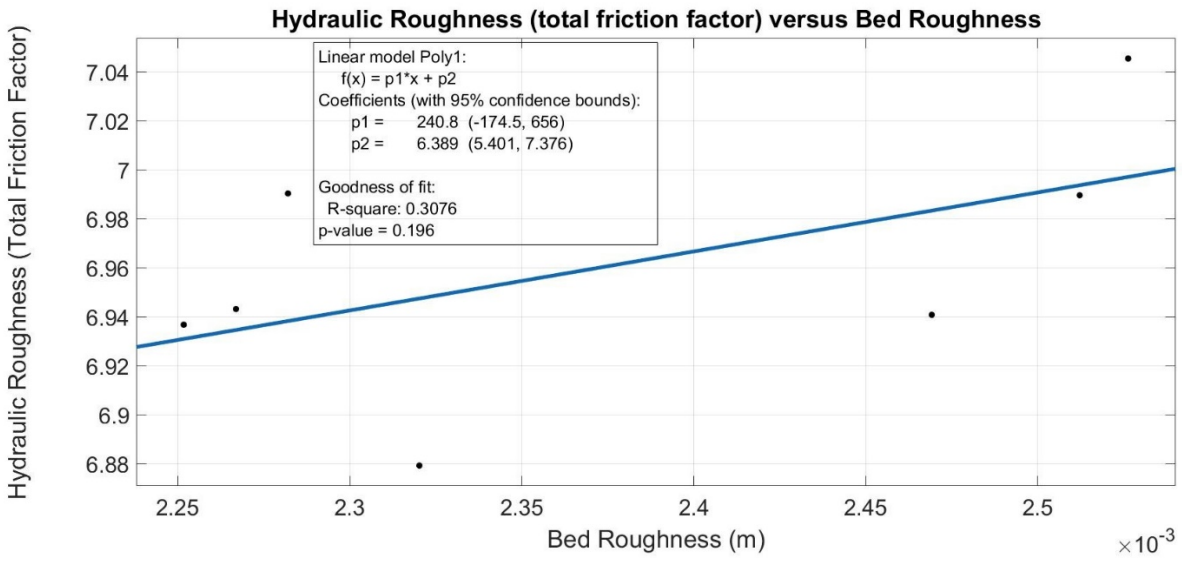

Figure 9: Hydraulic roughness (total friction factor) versus bed roughness for time steps 13 through 22.

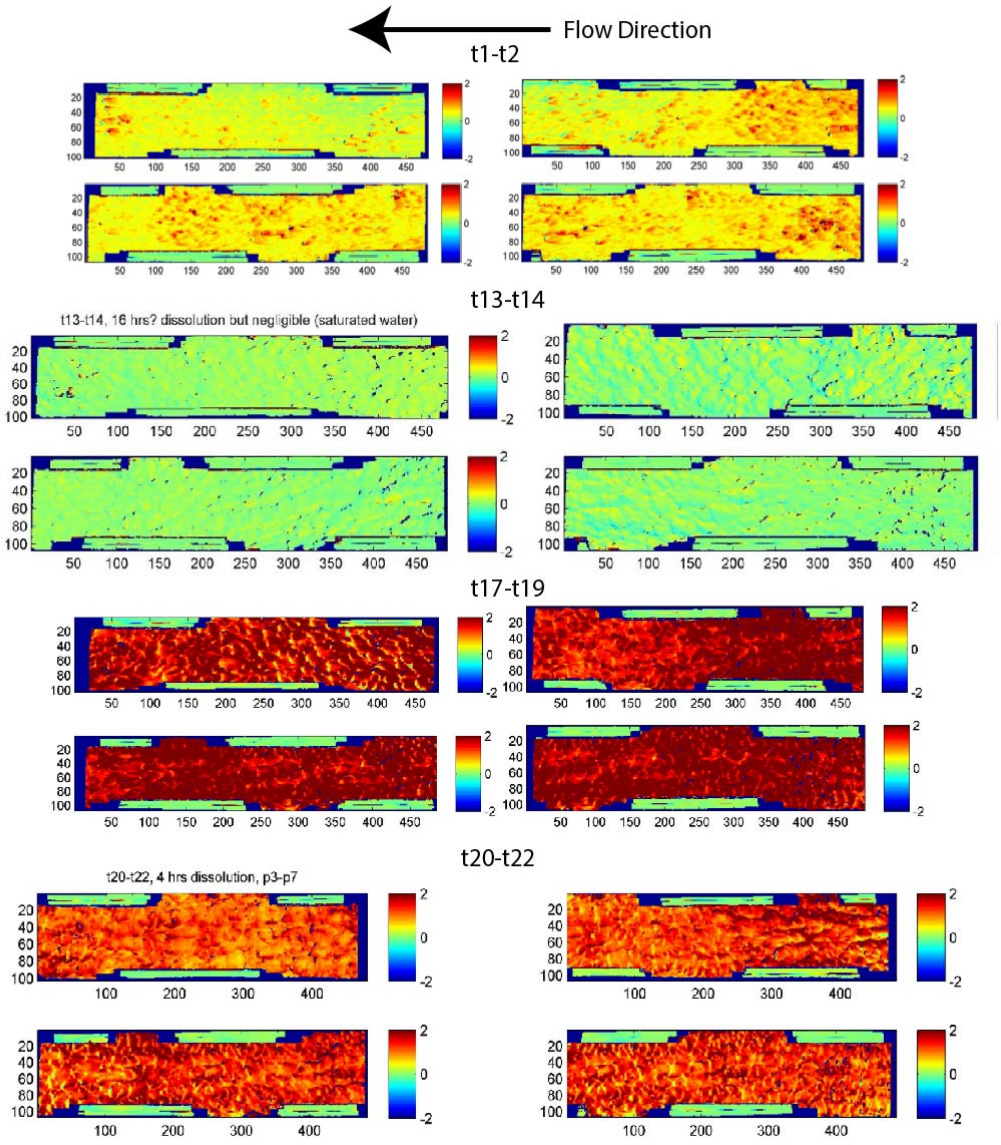

Figure 10: Erosion difference maps between time steps 1 and 2 (4hr dissolution), time steps 13 and 14 (16 hrs of dissolution in saturated water), time steps 17 and 19 (16hrs dissolution in water under saturated with respect to gypsum), and time steps 20 and 22 (4 hrs of dissolution with water under saturated with respect to gypsum). Color bar scale is in mm and hot colors represent areas of higher erosion.

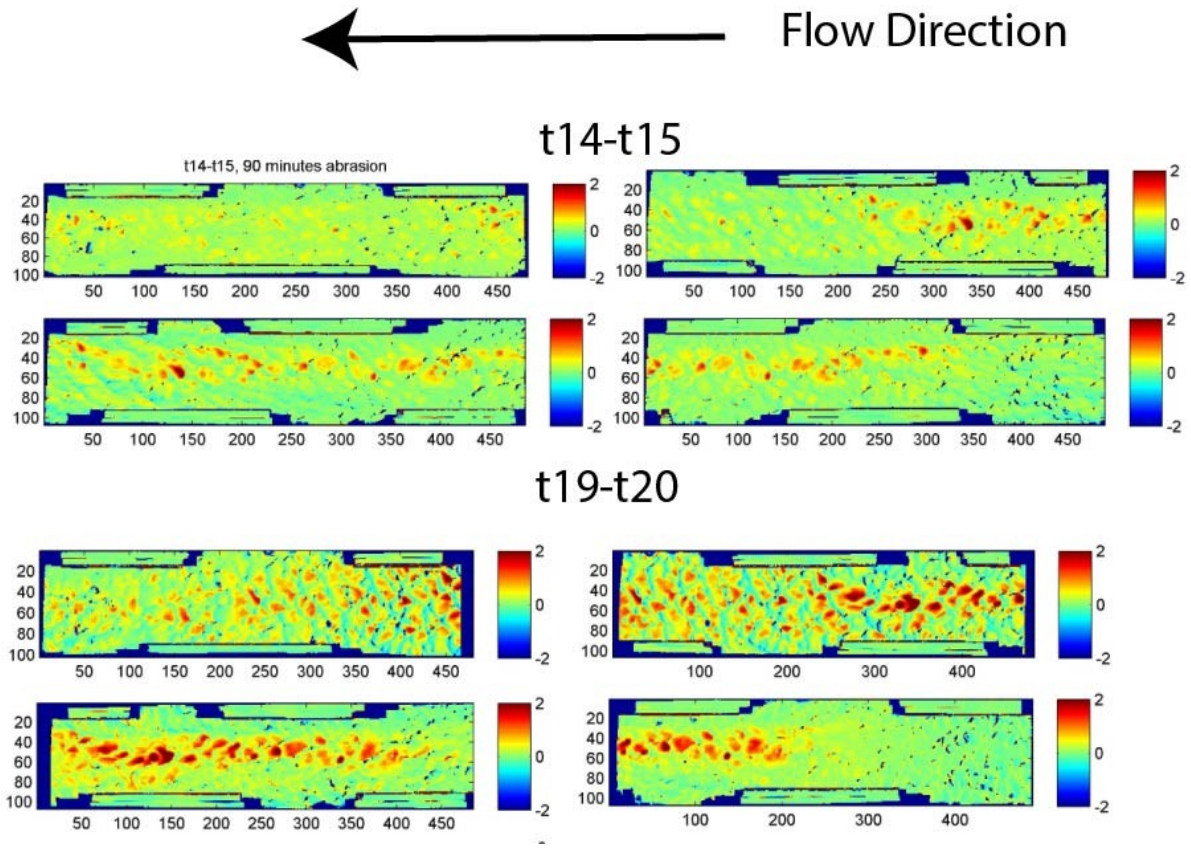

Figure 11: Erosion difference maps between time steps 14 and 15 (90min of abrasion) and time steps 19 and 20 (180min abrasion). Color bar scale is in mm and hot colors represent areas of higher erosion.

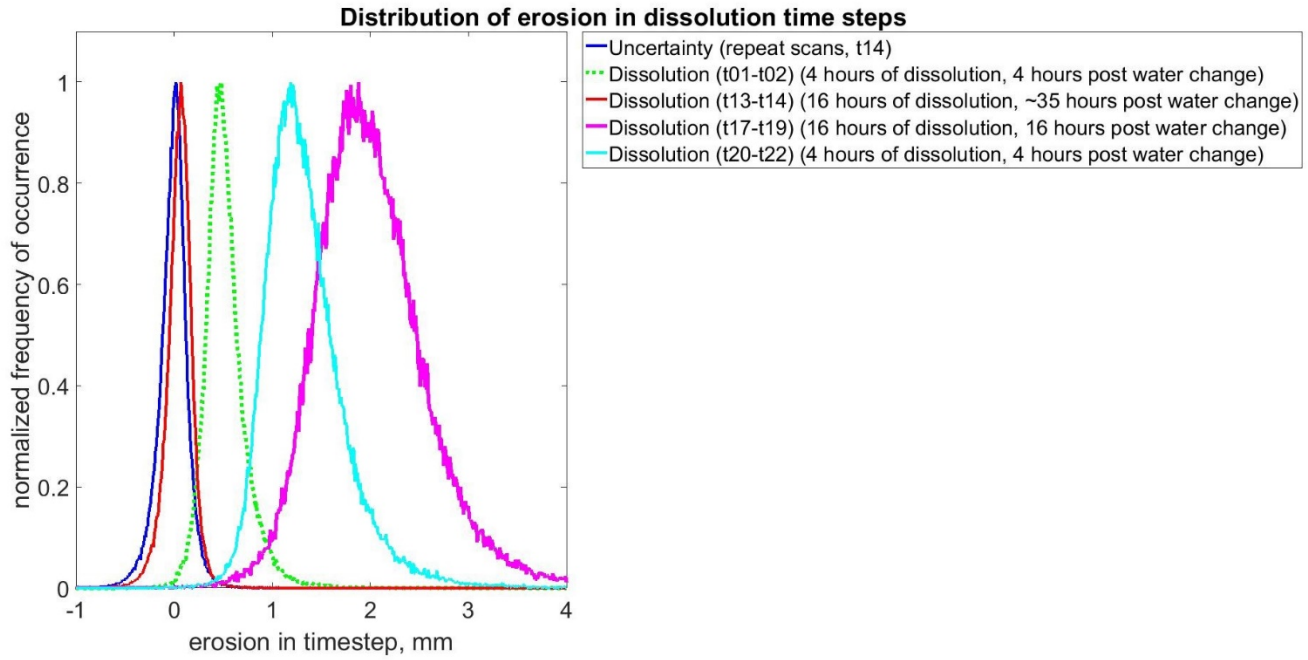

Figure 12: Erosion for dissolution time steps fit to normal distribution curves.

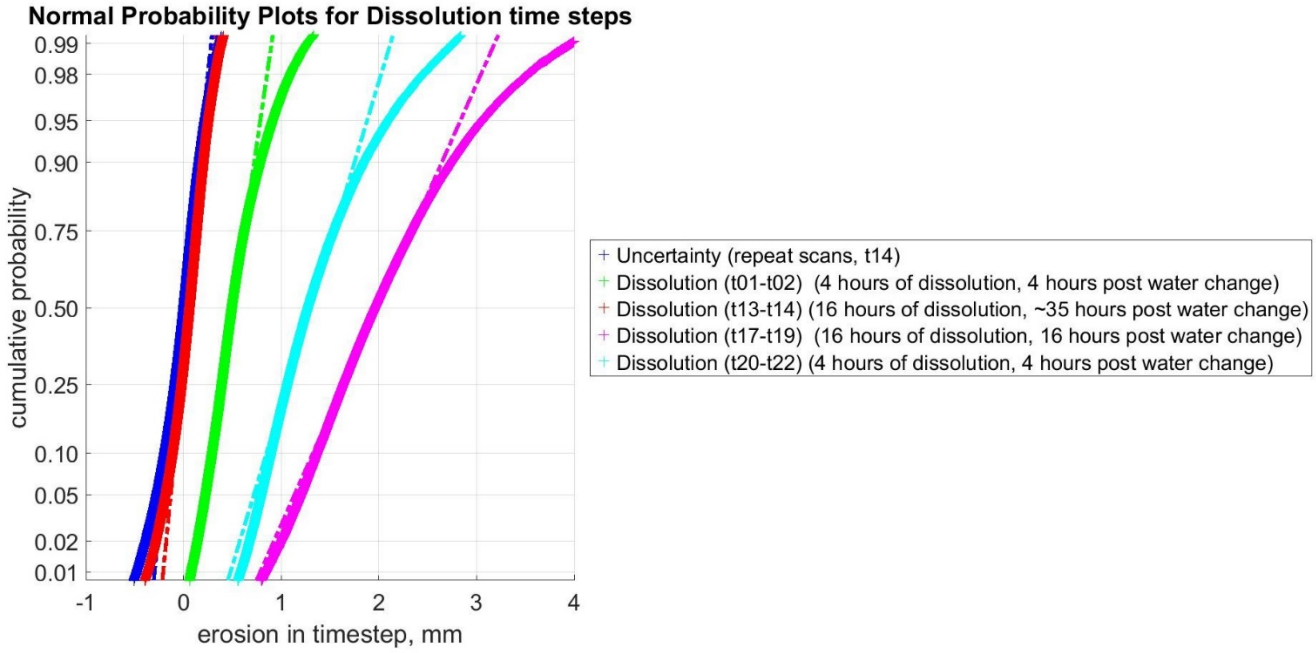

Figure 13: Normal probability plots for cumulative erosion of dissolution time steps.

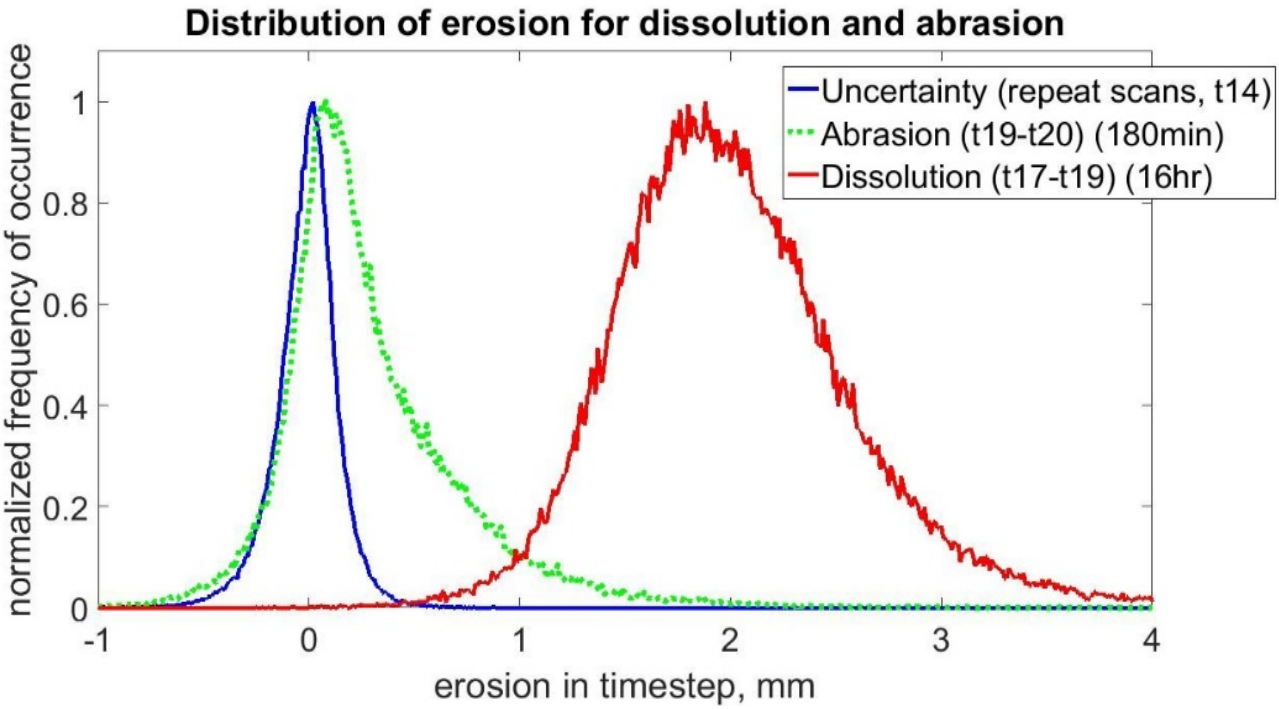

Figure 14: Distribution of cumulative erosion for 16hr of dissolution (t17-t19) followed by 180min of abrasion (t19-t20).

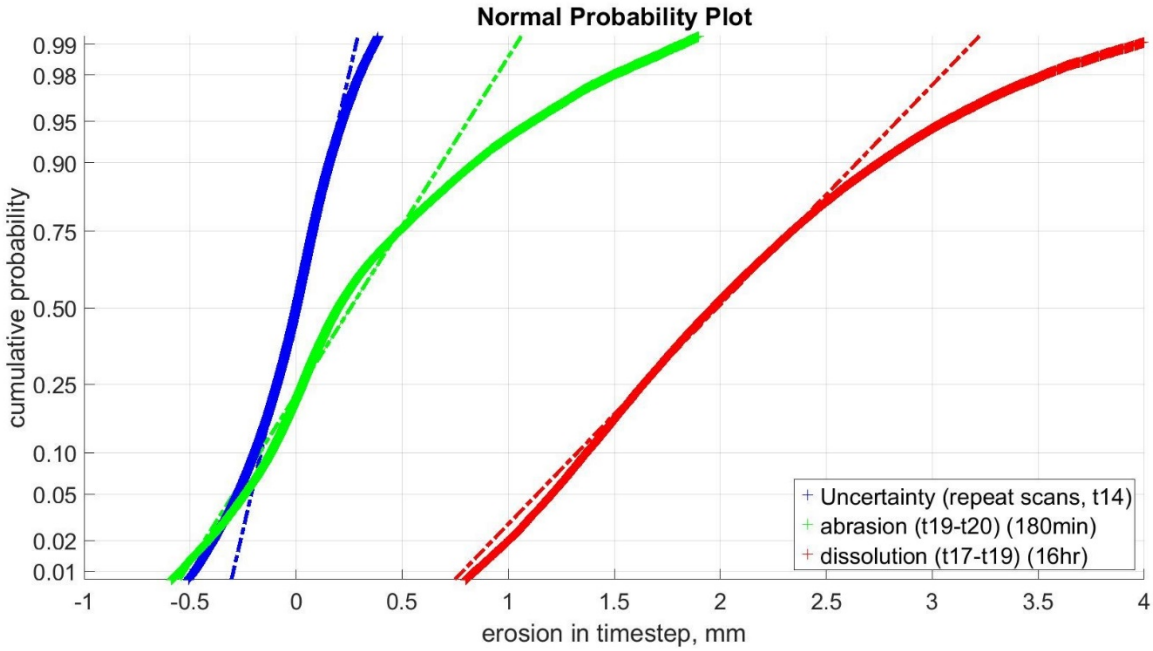

Figure 15: Normal probability plots for cumulative erosion of dissolution (t17-t19) and abrasion time steps (t19-t20).

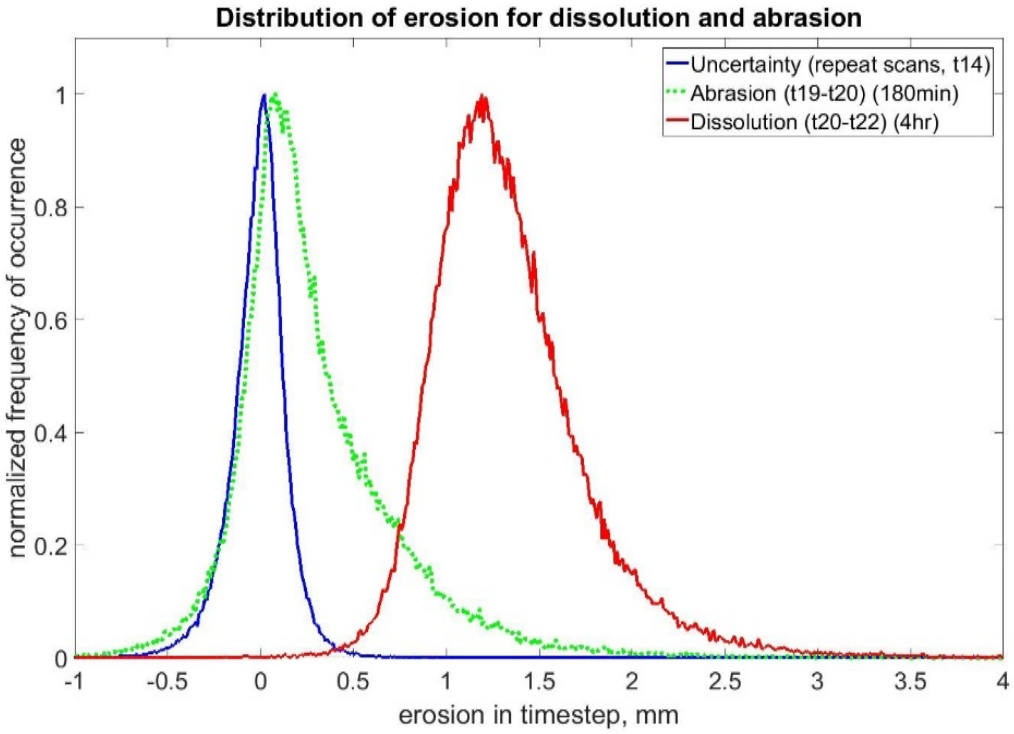

Figure 16: Distribution of cumulative erosion for 180min of abrasion (t19-t20) followed by 4hrs of dissolution (t20-t22).

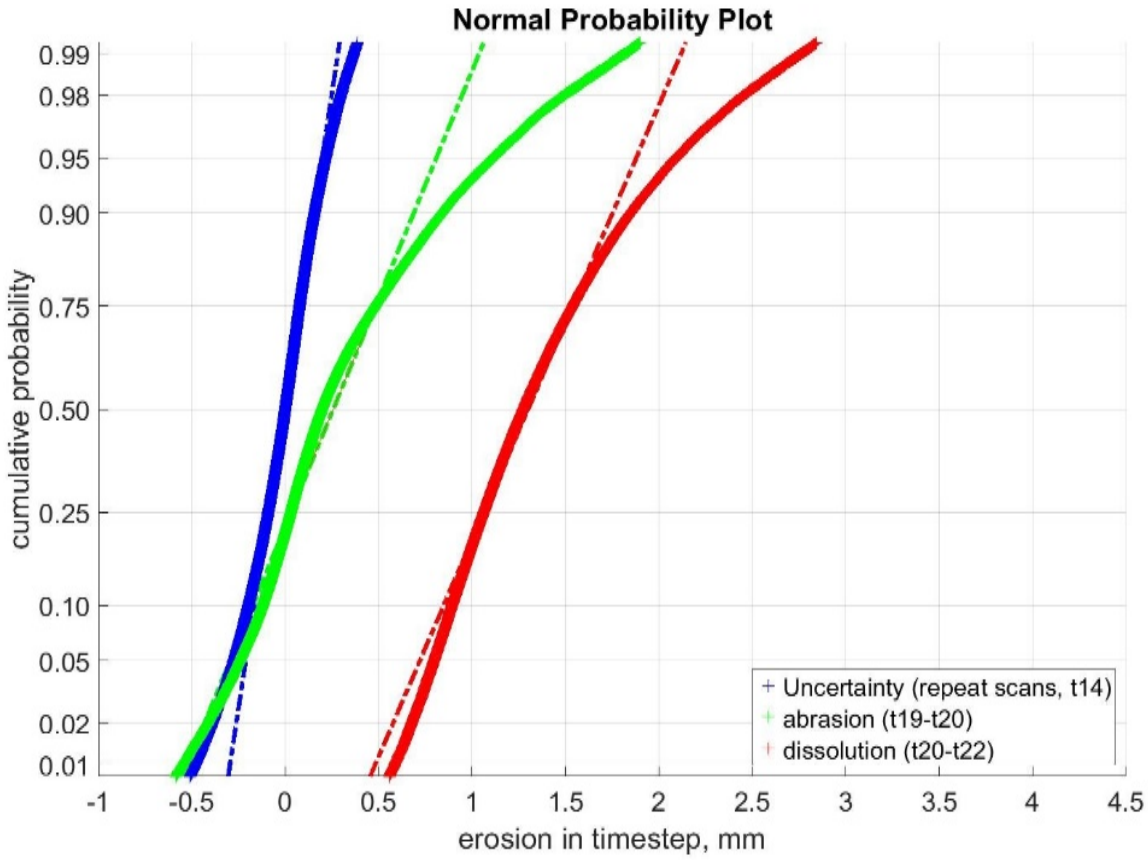

Figure 17: Normal probability plots for cumulative erosion of abrasion (t19-t20) and dissolution (t20-t22) time steps.

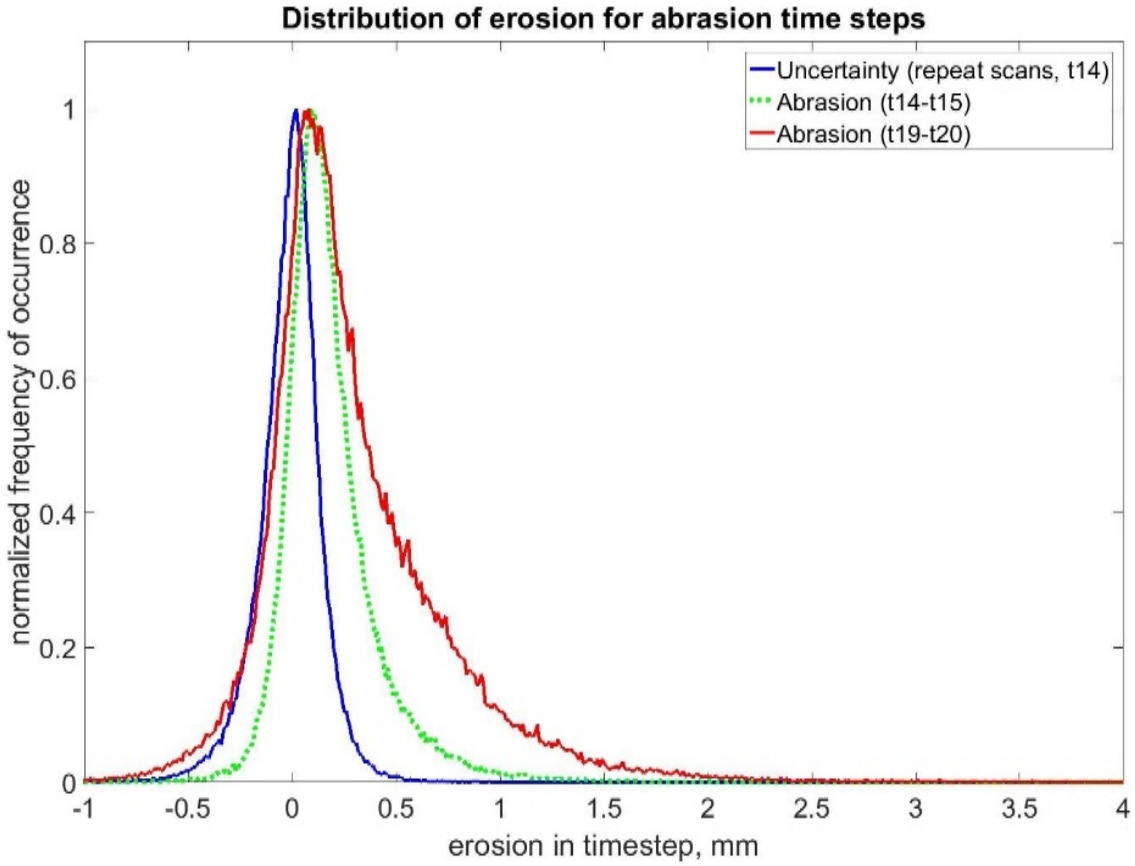

Figure 18: Erosion for abrasion time steps fit to normal distribution curves.

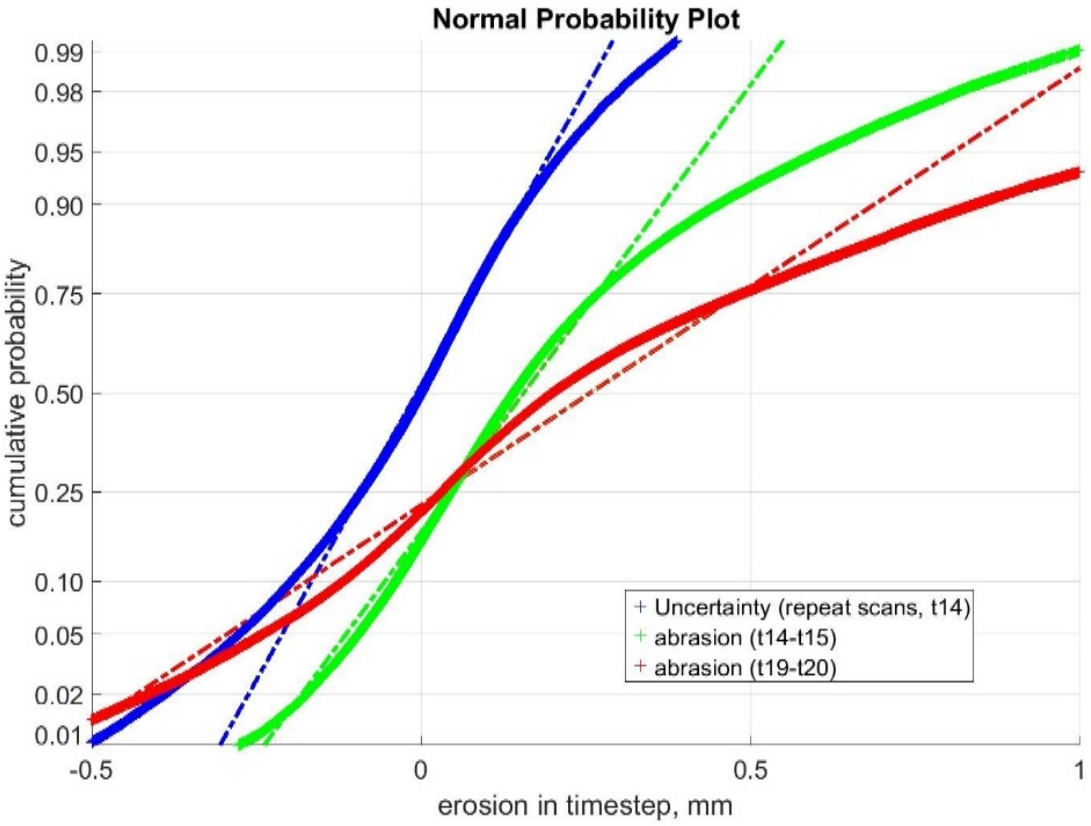

Figure 19: Normal probability plots for cumulative erosion of abrasion time steps.

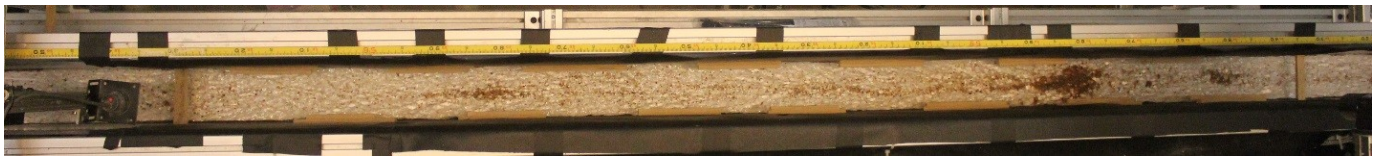

Figure 20: Image of flume bed from overhead camera during an abrasion time step. Sediment is seen to be mainly transported in the center of the flume bed.

Time step	Median (mm)	IQR (mm)	Erosion Rate (mm/hr)	Average Conductivity (mS/cm)
t1-t2	0.4945	0.2296	0.1624	1.1051
t13-t14	0.0611	0.153549	0.0033	2.6417
t14-t14	2.15E-04	0.167641	N/A	N/A
t14-t15	0.1404	0.22145	0.0816	2.6063
t15-t17	0.1258	0.233118	0.1003	2.6935
t17-t19	1.9623	0.695469	0.1406	2.0123
t19-t20	0.1977	0.452915	0.1624	1.1051
t20-t22	1.2736	0.474901	0.3575	1.2062

Table 2: Median and interquartile range values for cumulative erosion of processed time steps.

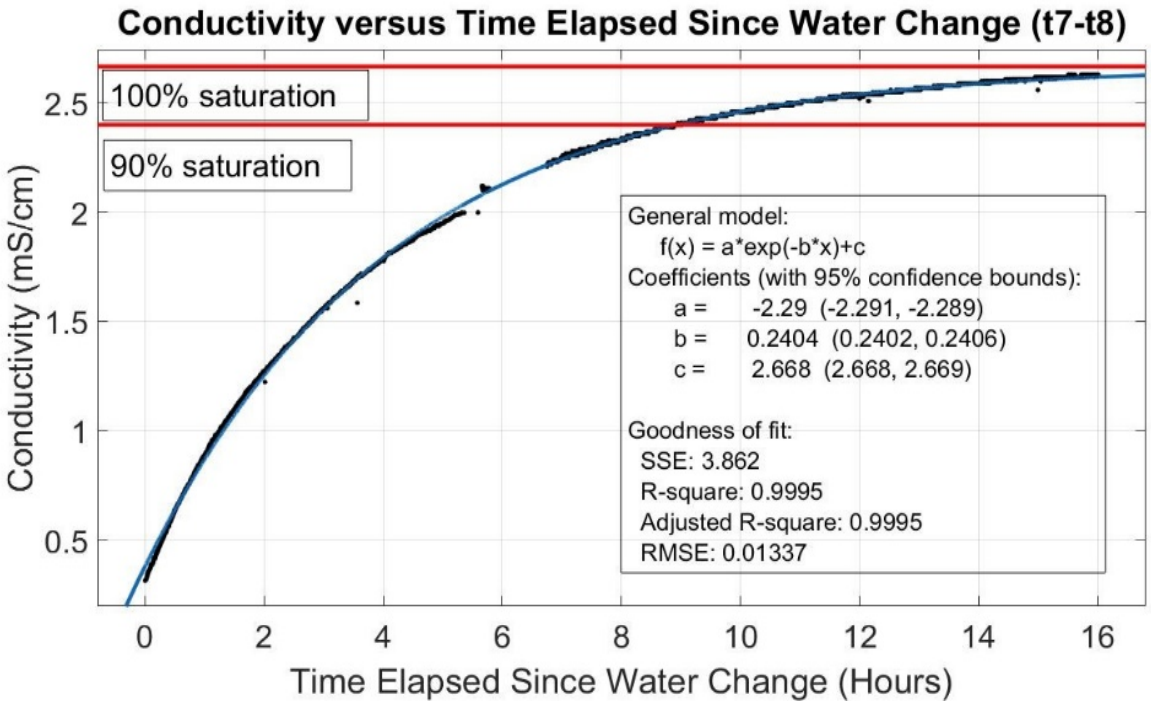

Figure 21: Conductivity versus time plot between time steps 7 and 8 showing the lines of 100 and 90 percent saturation state.

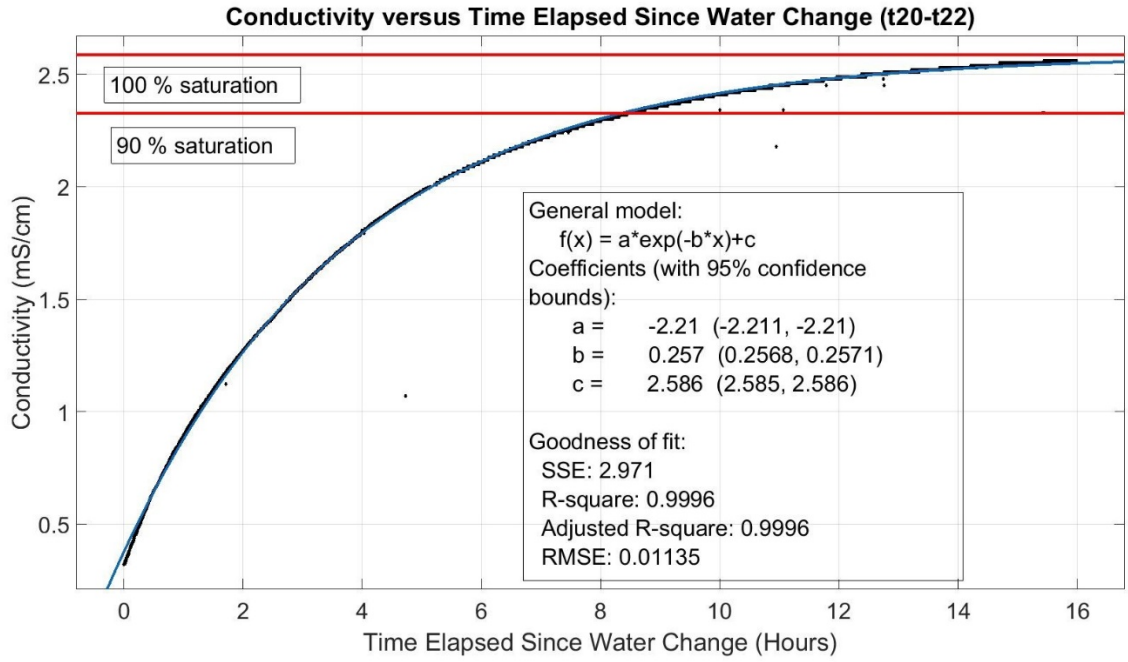

Figure 22: Conductivity versus time plot between time steps 20 and 22 showing the lines of 100 and 90 percent saturation state.

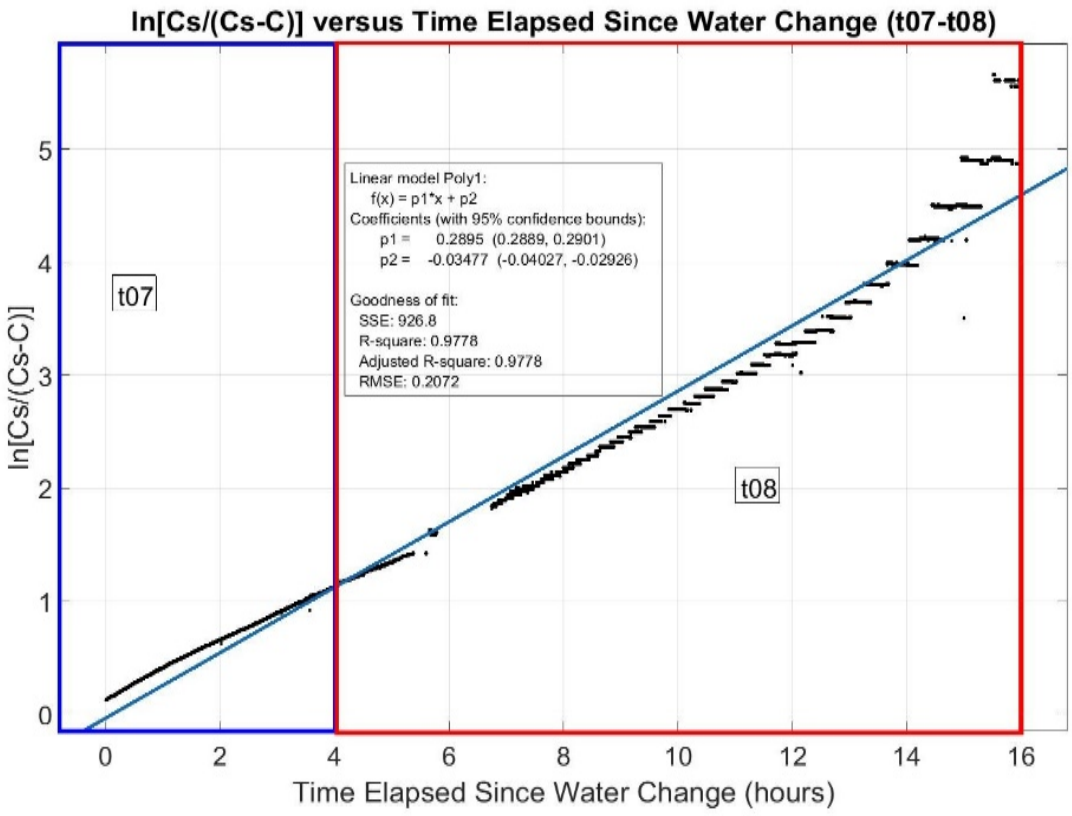

Figure 23: Plot of $\ln[C_s/(C_s-C)]$ versus elapsed time for 16hrs of dissolution between time steps 7 and 8.

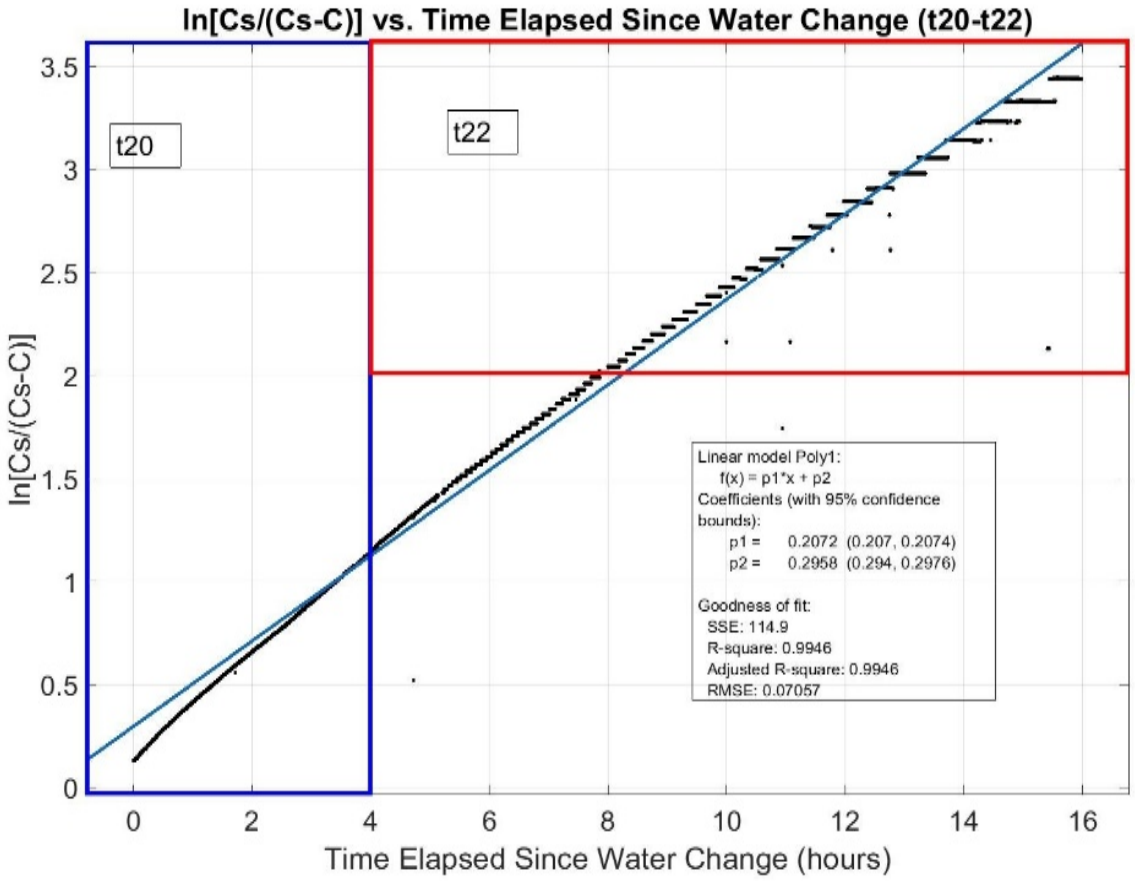

Figure 24: Plot of $\ln[C_s/(C_s-C)]$ versus elapsed time for 16hrs of dissolution between time steps 20 and 22.

References

Allen, J.R.L., 1966, Note on the use of plaster of paris in flow visualization, and some geological applications: Journal of Fluid Mechanics, v. 25, p. 331–335.

Allen, J.R.L., 1971, Transverse erosional marks of mud and rock: their physical basis and geological significance: Sedimentary Geology, v. 5, p. 167–385, doi: 10.1016/0037-0738(71)90001-7.

Baird, M.E., and Atkinson, M.J., 1997, Measurement and prediction of mass transfer to experimental coral reef communities: Limnology and Oceanography, v. 42, p. 1685–1693, doi: 10.4319/lo.1997.42.8.1685.

Barton, A.F.M., and Wilde, N.M., 1971, Dissolution rates of polycrystalline samples of gypsum and orthorhombic forms of calcium sulphate by a rotating disc method: Transactions of the Faraday Society, v. 67, p. 3590–3597, doi: 10.1039/TF9716703590.

Comiti, F., Cadol, D., and Wohl, E., 2009, Flow regimes, bed morphology, and flow resistance in self-formed step-pool channels: Water Resources Research, v. 45, p. W04424, doi: 10.1029/2008WR007259.

Covington, M.D. Natural variations in calcite dissolution rates in streams: Controls, implications, and open: Geophysical Research Letters, v. 42, p. 2836–2843.

Falter, J.L., Atkinson, M.J., Lowe, R.J., Monismith, S.G., and Koseff, J.R., 2007, Effects of nonlocal turbulence on the mass transfer of dissolved species to reef corals: Limnology and Oceanography, v. 52, p. 274–285, doi: 10.4319/lo.2007.52.1.0274.

Finnegan, N.J., Sklar, L.S., and Fuller, T.K., 2007, Interplay of sediment supply, river incision, and channel morphology revealed by the transient evolution of an experimental bedrock channel: Journal of Geophysical Research: Earth Surface, v. 112, p. F03S11, doi: 10.1029/2006JF000569.

Goodchild, M.F., and Ford, D.C., 1971, Analysis of Scallop Patterns by Simulation under Controlled Conditions: The Journal of Geology, v. 79, p. 52–62, doi: 10.2307/30060831.

Hearn, C., Atkinson, M., and Falter, J., 2001, A physical derivation of nutrient-uptake rates in coral reefs: effects of roughness and waves: Coral Reefs, v. 20, p. 347–356, doi: 10.1007/s00338-001-0185-6.

Hem, J.D., 1985, Study and Interpretation of the Chemical Characteristics of Natural Water: U.S. Geological Survey Water-Supply Paper 2254.

James, A.N., 1992, Soluble materials in civil engineering: Ellis Horwood Limited, 448 p.

Jeschke, A.A., Vosbeck, K., and Dreybrodt, W., 2001, Surface controlled dissolution rates of gypsum in aqueous solutions exhibit nonlinear dissolution kinetics: Geochimica et Cosmochimica Acta, v. 65, p. 27–34, doi: 10.1016/S0016-7037(00)00510-X.

Johnson, J.P.L., and Whipple, K.X., 2007, Feedbacks between erosion and sediment transport in experimental bedrock channels: Earth Surface Processes and Landforms, v. 32, p. 1048–1062, doi: 10.1002/esp.1471.

Johnson, J.P.L., and Whipple, K.X., 2010, Evaluating the controls of shear stress, sediment supply, alluvial cover, and channel morphology on experimental bedrock incision rate: Journal of Geophysical Research: Earth Surface, v. 115, p. F02018, doi: 10.1029/2009JF001335

Johnson, J.P.L., 2014, A surface roughness model for predicting alluvial cover and bed load transport rate in bedrock channels: Journal of Geophysical Research: Earth Surface, v. 119, p. 2147–2173.

Kirchner, J., Dietrich, W.E., Iseya, F., and Ikeda, H., 1990, The variability of critical shear stress, friction angle, and grain protrusion in water-worked sediments: Sedimentology, v. 37, p. 647–672.

Klimchouk, A., 1996, The dissolution and conversion of gypsum and anhydrite: International Journal of Speleology, v. 25, doi: http://dx.doi.org/10.5038/1827-806X.25.3.2 .

Nelson, P.A., and Seminara, G., 2012, A theoretical framework for the morphodynamics of bedrock channels: Geophysical Research Letters, v. 39, p. L06408, doi: 10.1029/2011GL050806.

Parker, G., 2007, Physical basis for quasi-universal relations describing bankfull hydraulic geometry of single-thread gravel bed rivers: Journal of Geophysical Research: Earth Surface, v. 112, http://onlinelibrary.wiley.com/doi/10.1029/2006JF000549/full (accessed August 2017).

Parker, G., 1991, Selective Sorting and Abrasion of River Gravel. I: Theory: Journal of Hydraulic Engineering, v. 117, p. 131–147, doi: 10.1061/(ASCE)0733-9429(1991)117:2(131).

Richardson, K., and Carling, P., 2005, A Typology of Sculpted Forms in Open Bedrock Channels: Geological Society of America, 116 p.

Ryb, U., Matmon, A., Erel, Y., Haviv, I., Benedetti, L., and Hidy, A.J., 2014, Styles and rates of long-term denudation in carbonate terrains under a Mediterranean to hyper-arid climatic gradient: Earth and Planetary Science Letters, v. 406, p. 142–152, doi: 10.1016/j.epsl.2014.09.008.

Ryb, U., Matmon, A., Haviv, I., and Benedetti, L., 2015, Exhumation and uplift coupled with precipitation along the western Dead Sea Rift margin: Geology, v. 43, p. 483–486, doi: 10.1130/G36331.1.

Sklar, L.S., and Dietrich, W.E., 2001, Sediment and rock strength controls on river incision into bedrock: Geology, v. 29, p. 1087–1090, doi: 10.1130/0091-7613(2001)029<1087:SARSCO>2.0.CO;2.

Thompson, T.L., and Glenn, E.P., 1994, Plaster standards to measure water motion: Limnology and Oceanography, v. 39, p. 1768–1779, doi: 10.4319/lo.1994.39.7.1768.

Turowski, J.M., Hovius, N., Meng-Long, H., Lague, D., and Men-Chiang, C., 2008, Distribution of erosion across bedrock channels: Earth Surface Processes and Landforms, v. 33, p. 353–363, doi: 10.1002/esp.1559.

Vita

Juliana Jennifer Spector was born in 1988 in Oakland, California. Juliana attended elementary, junior high, and high school in Oakland. She went on to study at the University of California, Berkeley in Berkeley, CA where she graduated with a Bachelor of Arts degree in Geology. Following four combined years of working as a hydrologic technician for the United States Geological Survey in Sacramento, CA and as a geologist for the Bureau of Safety and Environmental Enforcement in Camarillo, CA, Juliana resumed higher education to pursue a Master of Science degree at The University of Texas at Austin. She researched the geomorphology of carbonate bedrock incision in channels, with a particular focus on distinguishing chemical and physical erosion processes.

Permanent email: jjspector@utexas.edu

This thesis was typed by Juliana Jennifer Spector.